a high-fat, high-sucrose diet (HFHSD) that is known to induce obesity, insulin resistance, and steatosis (Maeda et al., 2002). HFHSD tended to induce body weight gains in wild-type and *Sepp1*-deficient mice, although there was no significance between the three groups of animals (Figure 6A). Daily food intake was significantly increased in *Sepp1*$^{-/-}$ mice compared with wild-type animals (Figure 6B). Basal energy expenditure, as measured by O_2 consumption through indirect calorimetry, was also increased in *Sepp1*$^{-/-}$ mice (Figure 6C). Liver triglyceride content and epididymal fat mass were unaffected by *Sepp1* gene deletion (Figures S4A and 6D). However, diet-induced hypertrophy of adipocytes was attenuated in *Sepp1*$^{-/-}$ mice (Figures 6E and 6F and Figure S4B). Additionally, serum levels of free fatty acid and insulin were significantly reduced in these animals (Figures 6G–6I). Glucose and insulin loading tests revealed that *Sepp1*$^{-/-}$ mice were protected against glucose intolerance and insulin resistance even when on an obesity-inducing diet (Figures 6J and 6K).

SeP Reduces Phosphorylation of AMPKα Both In Vitro and In Vivo

Adenosine monophosphate-activated protein kinase (AMPK) is a serine/threonine kinase that phosphorylates a variety of energy-associated enzymes and functions as a metabolic regulator that promotes insulin sensitivity (Kahn et al., 2005). In this study, we found that SeP treatment reduced phosphorylation of AMPKα and ACC in both H4IIEC hepatocytes and mouse liver (Figures S5A and 7A). Fatty acid β oxidation and β oxidation-related gene expression were also suppressed by SeP (Figures S5B–S5D). The levels of AMP and ATP were unchanged in hepatocytes treated with SeP (Figure S5E). In contrast, *Sepp1*-deficient mice exhibited increased phosphorylation of AMPKα and ACC in the liver (Figure 7B). To determine whether AMPK pathways were involved in the action of SeP, we infected H4IIEC hepatocytes with an adenovirus encoding dominant-negative (DN) or constitutively active (CA) AMPK. Transduction with DN-AMPK reduced insulin-stimulated Akt phosphorylation such that it could not be further decreased by SeP (Figures 7C–7E). In contrast, when CA-AMPK was overexpressed, SeP was unable to impair insulin-stimulated Akt phosphorylation (Figures 7F–7H). Additionally, coadministration of 5-aminoimidazole-4-carboxyamide ribonucleoside (AICAR), a known activator of AMPK, rescued cells from the inhibitory effects of SeP on insulin signaling (Figure 7I). These results suggest that reduced phosphorylation of AMPK mediates, at least in part, the inhibitory effects of SeP on insulin signal transduction. Next, we examined the effects of SeP on some of the proteins that regulate the phosphorylation of AMPK. SeP dose-dependently increased the levels of protein phosphatase 2C (PP2C), a negative regulator of AMPK phosphorylation, in H4IIEC hepatocytes (Figure 7J). Expression of LKB1 and CaMKKβ, two positive regulators of AMPK, was unaffected by SeP treatment.

DISCUSSION

A Liver-Derived Secretory Protein, SeP, Causes Insulin Resistance

Our research reveals that hepatic overproduction of SeP contributes to the development of insulin resistance in the liver and skeletal muscle (Figure S5F). The liver plays a central role in glucose homeostasis, mainly via glycogen storage and glucose release into the blood stream. In addition, the liver is a major site for the production of secretory proteins. Therefore, we hypothesized that the liver would maintain glucose homeostasis by producing liver-derived secretory protein(s) termed hepatokines. In fact, several studies have shown that hepatic secretory factors, including the angiopoietin-like protein family (Oike et al., 2005; Xu et al., 2005) and fetuin-A (Auberger et al., 1989; Srinivas et al., 1993), are involved in insulin sensitivity. However, we speculated that the identification of the liver-derived proteins that directly contribute to the pathogenesis of insulin resistance or type 2 diabetes may not be adequate. Specifically, our comprehensive approach using global gene expression analyses revealed that numerous genes encoding secretory proteins are expressed and altered in the human type2 diabetic liver (Misu et al., 2007). Thus, by comparing the expression levels and clinical parameters for glycemic control and insulin resistance, we selected candidate genes for liver-produced secretory proteins that cause insulin resistance. The current study sheds light on a previously underexplored function of the liver that is similar to adipose tissue; the liver may participate in the pathogenesis of insulin resistance through hormone secretion.

Suppression of SeP Expression by Insulin in Hepatocytes

Our results indicate that insulin negatively regulates SeP expression in hepatocytes. These findings are consistent with recent reports that the SeP promoter is a target of FoxO (forkhead box, class O) and PGC-1α (peroxisome proliferator-activated receptor-γ coactivator 1α), both of which are negatively regulated by insulin in hepatocytes (Speckmann et al., 2008; Walter et al., 2008). Consistent with these findings in vitro, we showed that hepatic SeP expression was upregulated in mice in the fasting state. Under hypoinsulinemic conditions, such as a fasting state, upregulation of SeP might prevent hypoglycemia by decreasing glucose uptake in peripheral tissues and by increasing hepatic glucose production. Our results raise the possibility that the liver regulates systemic insulin sensitivity by sensing blood insulin levels and altering the production of SeP.

SeP Decreases Phosphorylation of AMPK and ACC in Hepatocytes

Identification of SeP receptor(s) in insulin-target organs is necessary to clarify the action mechanisms of SeP. Several lines of evidence have shown that apolipoprotein E receptor 2 (ApoER2) functions as an SeP receptor in the testis (Olson et al., 2007) and brain (Burk et al., 2007), both by acting as a cellular uptake receptor and by inducing intracellular signaling (Masiulis et al., 2009). It remains unknown whether ApoER2 acts as the SeP receptor in the liver or skeletal muscle. However, in this study, technical difficulties in the identification of a SeP receptor(s) led us to screen for well-established pathways associated with metabolic derangement to clarify the specific mechanisms of SeP action. As a result, our experiments reveal that SeP reduces phosphorylation of AMPK and its target ACC in H4IIEC hepatocytes and the livers of C57BL6J mice, possibly in an AMP/ATP ratio-independent manner. AMPK functions as a regulator of

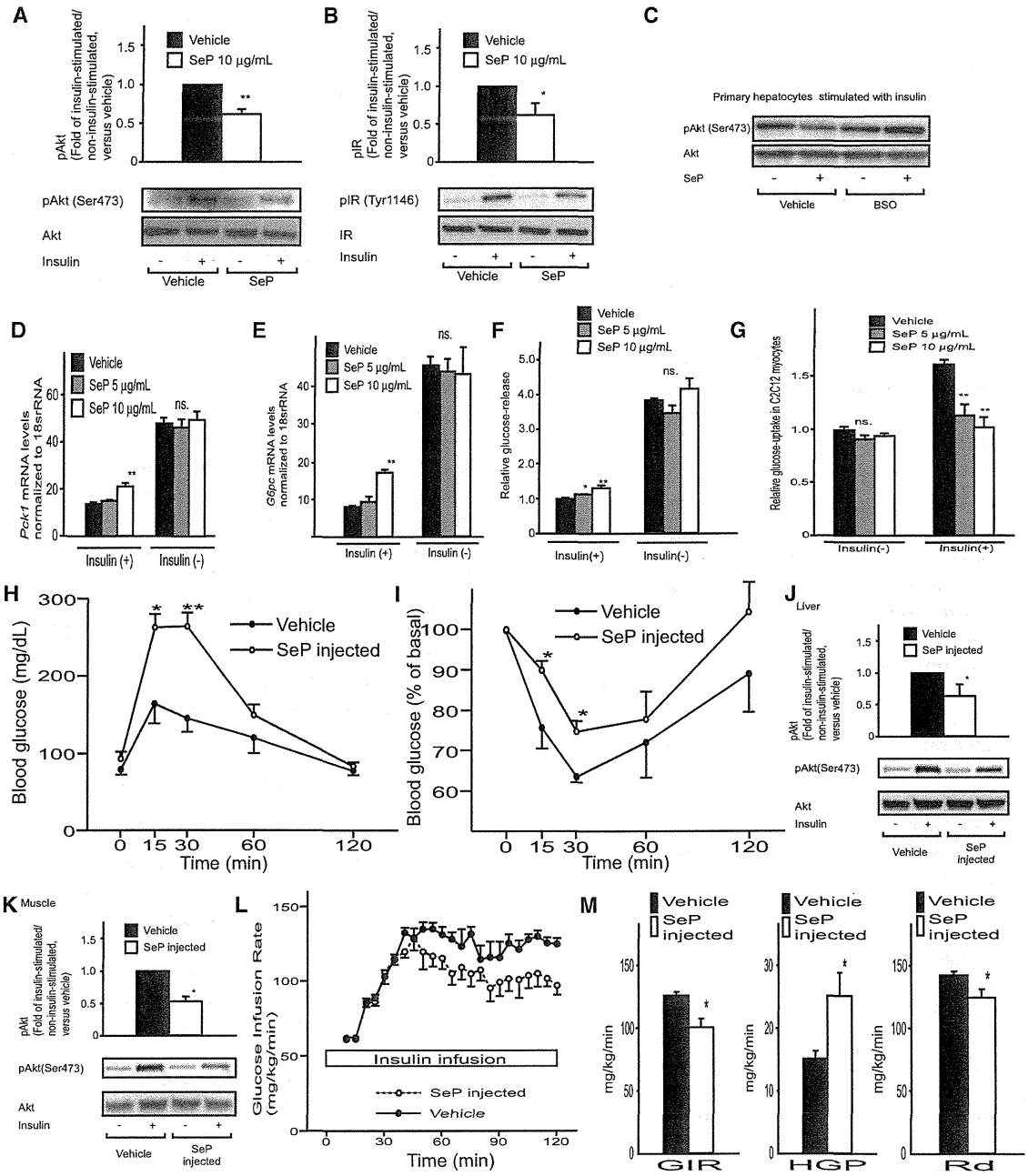

Figure 3. SeP Impairs Insulin Signaling In Vitro and In Vivo

(A and B) Effects of SeP on serine phosphorylation of Akt (A) and tyrosine phosphorylation of insulin receptor (B) in insulin-stimulated primary hepatocytes. Data represent the means ± SEM of three independent experiments. *$p < 0.05$, **$p < 0.01$ (versus vehicle-treated cells). Primary hepatocytes were treated with SeP or vehicle for 24 hr, and then the cells were stimulated with 1 ng/ml insulin for 15 min.

(C) Effects of BSO on SeP-induced changes in insulin-stimulated Akt phosphorylation in primary hepatocytes.

(D and E) Effects of SeP on the expression of mRNAs encoding gluconeogenic enzymes in H4IIEC hepatocytes (n = 5).

(F) Release of glucose from H4IIEC hepatocytes treated with SeP for 24 hr (n = 6).

(G) Effects of SeP on glucose uptake in C2C12 myocytes (n = 6).

(H and I) Glucose (H) and insulin (I) tolerance tests in mice injected with SeP or vehicle (n = 5). Glucose (1.5 g/kg body weight) and insulin (0.5 unit/kg body weight) were administered intraperitoneally.

(J and K) Effects of SeP on serine phosphorylation of Akt in liver (J) and skeletal muscle (K) in mice injected with purified human SeP or vehicle. Mice (n = 3 or 4) were stimulated with insulin (administered intraperitoneally). At 20 min after insulin stimulation, mice were anesthetized, and liver and hind-limb muscle samples removed for analysis.

(L) Time course of glucose infusion rate (GIR) during hyperinsulinemic-euglycemic clamp in mice injected with SeP or vehicle (n = 6).

(M) GIR, endogenous glucose production (EGP), and rate of glucose disposal (Rd) during hyperinsulinemic-euglycemic clamp (n = 6).

cellular energy homeostasis (Kahn et al., 2005) and mediates some effects of peripheral hormones such as leptin (Minokoshi et al., 2002) and adiponectin (Yamauchi et al., 2002); however, the mechanisms by which these adipokines alter AMPK phosphorylation are not fully understood. Our present findings demonstrate that SeP increases the levels of PP2C in H4IIEC hepatocytes. PP2C is a phosphatase that inactivates AMPK by dephosphorylating a threonine residue (Thr172) that lies in its α-catalytic subunit (Davies et al., 1995). Tumor necrosis factor α (TNF-α), a representative inflammatory cytokine linked to insulin resistance, is known to reduce AMPK phosphorylation by upregulating PP2C (Steinberg et al., 2006). Similar to TNF-α, SeP may reduce AMPK phosphorylation, at least partly, by upregulating PP2C. Further characterization of SeP and SeP-receptor-mediated interactions will provide insights into the involvement of SeP in PP2C upregulation and AMPK dephosphorylation.

Mechanism Underlying SeP-Mediated Insulin Resistance Varies between Liver and Skeletal Muscle

Given that plasma SeP is derived mainly from the liver (Carlson et al., 2004), our results suggest that AMPK mediates, at least in part, the autocrine/paracrine action of SeP. One limitation of our study is that the mechanism by which SeP acts on skeletal muscle remains unknown. Unlike in the liver, SeP-induced inhibitory effects on AMPK were not observed in either the skeletal muscle of C57BL6J mice or C2C12 myocytes (data not shown). Additionally, we showed that SeP reduces tyrosine phosphorylation of insulin receptors in primary hepatocytes. In contrast, SeP acts on serine phosphorylation of IRS1, but not tyrosine phosphorylation of insulin receptors, in C2C12 myocytes (data not shown). These results suggest that SeP disrupts the insulin signal cascade at different levels between hepatocytes and myocytes. SeP might induce insulin resistance in skeletal muscle, possibly through AMPK-independent pathways. The mechanisms that connect SeP to insulin resistance likely exhibit tissue specificity.

We showed that SeP heterozygous mice have no phenotype in glucose- and insulin-loading tests, whereas a 30% decrease in SeP levels caused by the injection of siRNA improves glucose tolerance and insulin resistance in KKAy mice. In general, multiple compensatory changes are observed in knockout mice, because the target gene has been absent since conception. In contrast, compensation may be inadequate in adult animals in which the target gene has been knocked down with siRNA. In fact, real-time PCR analysis showed that expression of the gene encoding IL-6, a representative inflammatory cytokine linked to insulin resistance, shows compensatory upregulation in the liver of *Sepp1*$^{-/+}$ mice, but not in *Sepp1* siRNA-treated KKAy mice (data not shown). Induction of IL-6 might compensate for the 50% reduction in SeP levels in *Sepp1*$^{-/+}$ mice.

Actions of SeP on the central nervous system may contribute to the in vivo phenotype. We did find that SeP-deficient mice fed a high-fat, high-sucrose diet display increases in food intake and O2 consumption (Figures 6B and 6C), suggesting that SeP acts on the central nervous system. Additionally, an earlier report described the colocalization of SeP and amyloid-β protein in the brains of people with Alzheimer's disease, suggesting the potential involvement of SeP in this condition's pathology (Bellinger et al., 2008). More recently, Takeda et al. reported that amyloid pathology in Alzheimer's disease may adversely affect diabetic phenotypes in mice (Takeda et al., 2010). Further experiments are necessary to determine whether the actions of SeP on the central nervous system involve the in vivo phenotype seen in this study.

We cannot exclude the possibility that the current phenotype in *Sepp1*-deficient mice is affected by the abnormal distribution of selenium. In fact, selenium levels in plasma and several tissues have been reported to be reduced in *Sepp1*-deficient mice fed a selenium-restricted diet (Schomburg et al., 2003). However, Burk et al. reported that the selenium levels in all tissues except the testis were unchanged in these mice fed a diet containing adequate amounts of selenium (Hill et al., 2003). In this study, we performed experiments using *Sepp1*-deficient mice fed a diet containing adequate amounts of selenium. Thus, we speculate that the effects of abnormal selenium distribution on our results in *Sepp1*-deficient mice may be insignificant.

A limitation of this study is that we could not match age, gender, or body weight completely between people with type 2 diabetes and normal subjects when comparing the serum SeP levels, as a result of the limited sample numbers. However, a previous large-scale clinical report showed that the age-, gender-, race-, and BMI-adjusted mean serum selenium levels were significantly elevated in participants with diabetes compared with those without diabetes in the US population (Bleys et al., 2007). Additionally, several lines of evidence showed that serum selenium levels are positively correlated with those of SeP in humans (Andoh et al., 2005; Persson-Moschos et al., 1998). In combination with our result, these reports lead us to speculate that serum SeP levels are also elevated in people with type 2 diabetes compared with normal subjects. However, additional large-scale clinical trials are needed to address this.

In summary, our experiments have identified SeP as a liver-derived secretory protein that induces insulin resistance and hyperglycemia. Our findings suggest that the secretory protein SeP may be a target for the development of therapies to treat insulin resistance-associated diseases, including type 2 diabetes.

EXPERIMENTAL PROCEDURES

Animals

Eight-week-old c57BL/6J mice were obtained from Sankyo Lab Service (Tokyo, Japan). Male Otsuka Long-Evans Tokushima Fatty (OLETF) rats and Long-Evans Tokushima Otsuka (LETO) rats were obtained from the Otsuka Pharmaceutical Tokushima Research Institute (Tokushima, Japan). OLETF

C57BL/6J mice were twice injected intraperitoneally with purified human SeP (1 mg/kg body weight) or vehicle in (H)–(M). Injections were administered 12 and 2 hr before the each experiment. Data in (D)–(G) represent the means ± SEM from five to six cells per group, and data in (H)–(M) represent the means ± SEM from three to six mice per group. *$p < 0.05$, **$p < 0.01$ versus cells treated with vehicle in (D)–(G). *$p < 0.05$, **$p < 0.01$ versus mice treated with vehicle in (H)–(M). See also Figure S1.

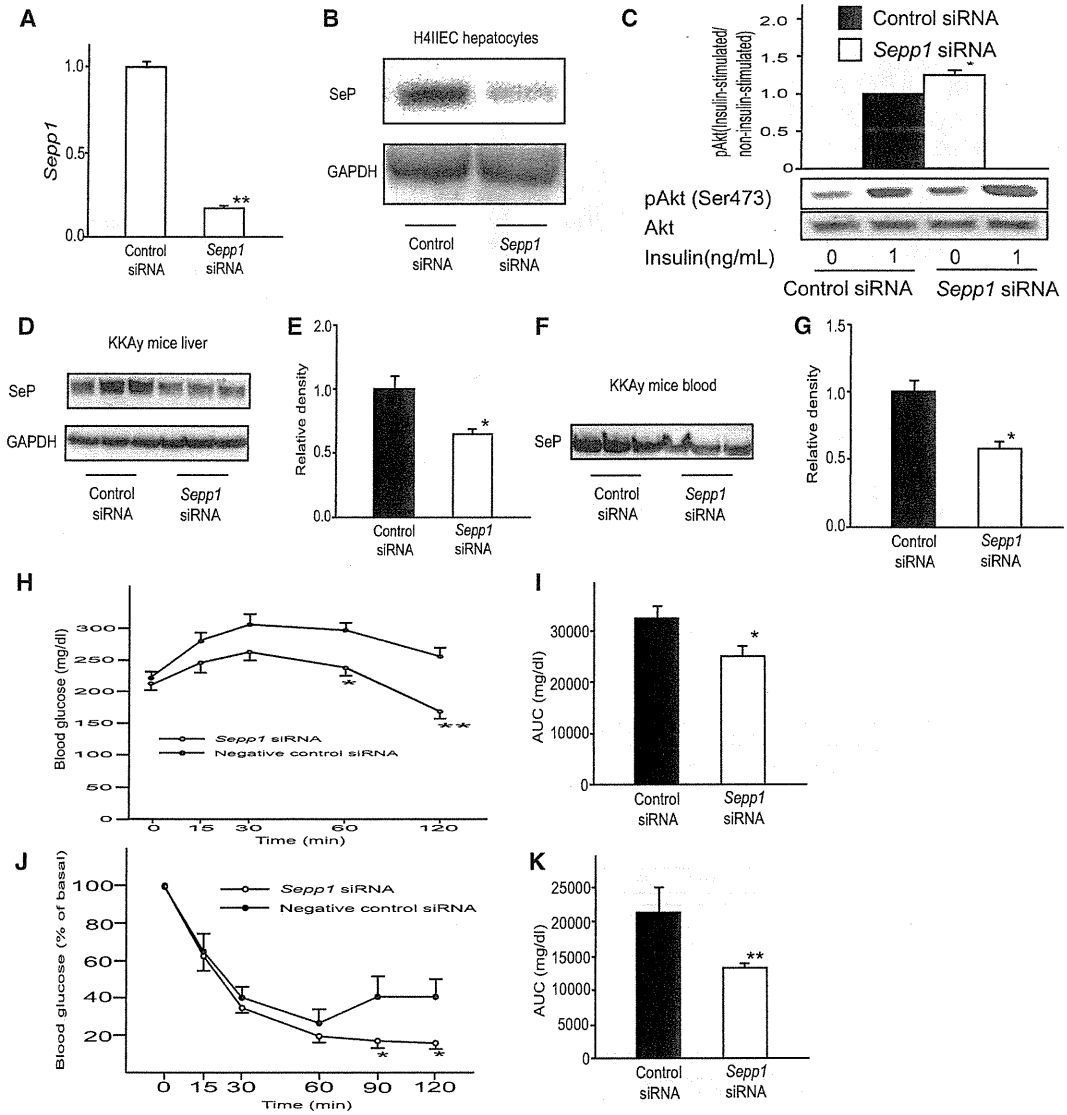

Figure 4. *Sepp1* Knockdown in the Liver Improves Insulin Sensitivity

(A) *Sepp1* mRNA levels in H4IIEC hepatocytes transfected with control or *Sepp1*-specific siRNA (n = 4).

(B) SeP protein production in H4IIEC hepatocytes transfected with *Sepp1*-specific siRNA. SeP production was detected in whole cell lysates by western blotting.

(C) Effects of SeP knockdown on insulin-stimulated serine phosphorylation of Akt in H4IIEC hepatocytes. Data represent the mean ± SEM of three independent experiments.

(D and E) Liver SeP production in KKAy mice injected with control or *Sepp1*-specific siRNA (n = 6). SeP protein levels were measured by western blotting 4 days after injection of siRNA.

(F and G) Blood SeP levels in KKAy mice injected with siRNA. Blood samples were obtained 4 days after siRNA injection (n = 6).

(H–K) Intraperitoneal glucose (H and I) and insulin (J and K) tolerance tests in KKAy mice (n = 6–8) injected with control or *Sepp1*-specific siRNA. Glucose and insulin was administered at doses of 0.3 g/kg body weight and 4 units/kg body weight, respectively.

Area under the curve (AUC) for blood glucose levels is shown in (I) and (K). Data in (A) represent the means ± SEM from four cells per group, and data in (E) and (G)–(K) represent the means ± SEM from six to eight mice per group. *$p < 0.05$ versus cells transfected with control siRNA in (A) and (C). *$p < 0.05$, **$p < 0.01$ versus mice injected with control siRNA in (E) and (G)–(K). See also Figure S2.

rats have been established as an animal model of obesity-related type 2 diabetes (Kawano et al., 1992). Female KKAy mice were obtained from CLEA Japan (Tokyo, Japan). All animals were housed in a 12 hr light/dark cycle and allowed free access to food and water. High-fat and high-sucrose diet (D03062301) was purchased from Research Diets (New Brunswick, NJ). The experiments with OLETF and LETO rats were performed with frozen blood and liver samples obtained in our previous study (Ota et al., 2007).

Purification of SeP

SeP was purified from human plasma via conventional chromatographic methods, as previously described (Saito et al., 1999; Saito and Takahashi, 2002). Homogeneity of purified human SeP was confirmed by analysis of both amino acid composition and sequence (Saito et al., 1999). Concentrations of purified SeP were measured by the Bradford method, using bovine immunoglobulin G as a standard.

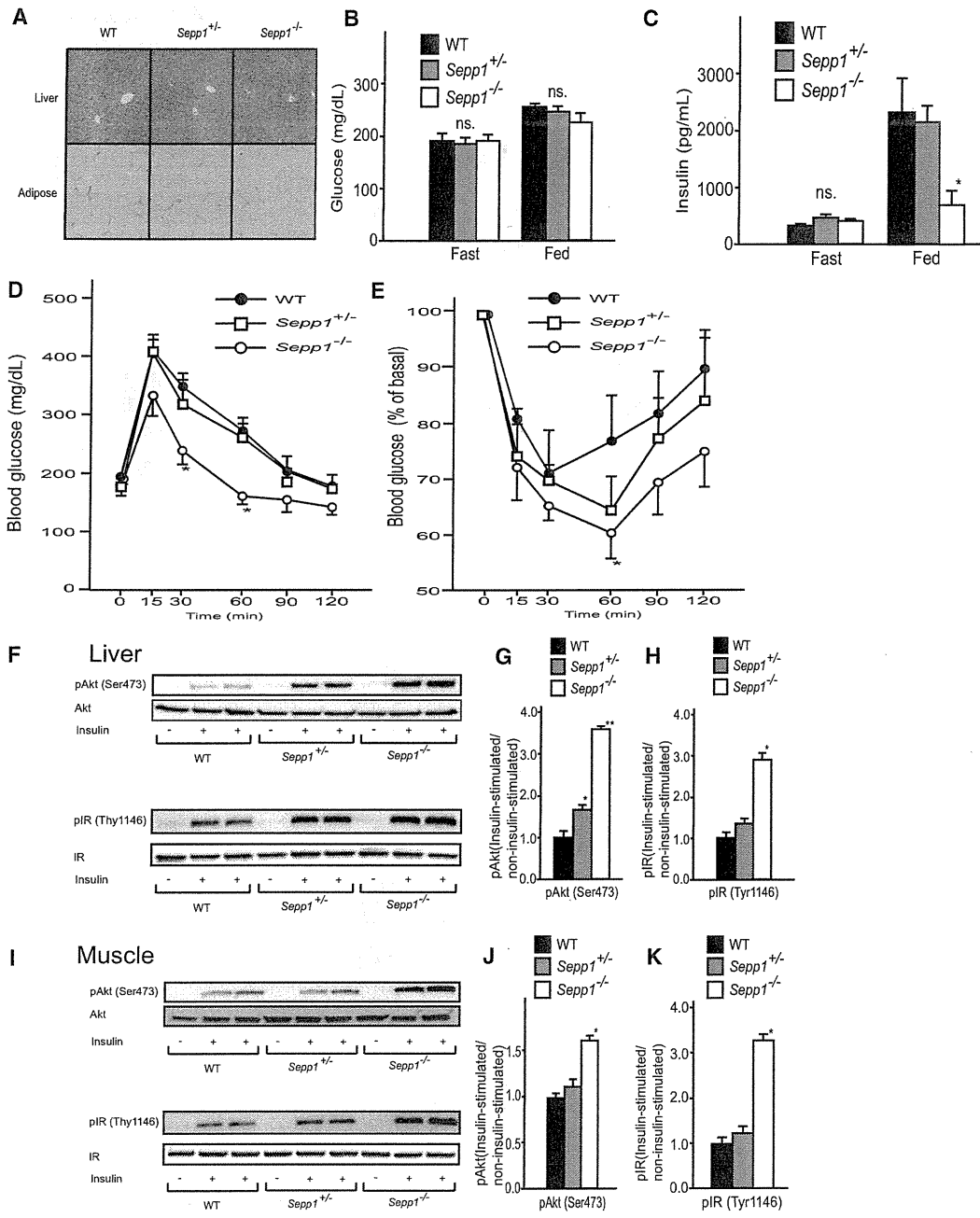

Figure 5. *Sepp1*-Deficient Mice Show Improved Glucose Tolerance and Enhanced Insulin Sensitivity

(A) Hematoxylin-and-eosin-stained liver and epididymal fat sections from male *Sepp1*$^{+/-}$ and *Sepp1*$^{-/-}$ mice.

(B) Blood glucose levels in *Sepp1*-deficient mice (n = 7). The mice were fasted for 6 hr.

(C) Blood insulin levels in *Sepp1*-deficient mice (n = 7).

(D and E) Intraperitoneal glucose (D) and insulin (E) tolerance tests in male *Sepp1*-deficient mice (n = 7). Glucose and insulin were administered at doses of 1.5 g/kg body weight and 4 units/kg body weight, respectively.

(F–K) Western blot analysis of phosphorylated Akt (pAkt) and phosphorylated insulin receptor (pIR) in liver (F–H) and skeletal muscle (I–K). Mice (n = 6) were stimulated with insulin (administered intraperitoneally). At 20 min after insulin stimulation, mice were anesthetized, and liver and hind-limb muscle samples removed for analysis.

Data in (B)–(E), (G), (H), (J), and (K) represent the means ± SEM from six to seven mice per group. *$p < 0.05$, **$p < 0.01$ versus wild-type mice. See also Figure S3.

siRNA Injection into KKAy mice

Delivery of siRNA targeted to the liver was performed by tail vein injections into mice, via hydrodynamic techniques, as previously described (McCaffrey et al., 2002; Zender et al., 2003). For these experiments, KKAy mice at 7–8 weeks of age (31–33 g body weight) were used. Mice were anesthetized with pentobarbital, and 2 nmol of siRNA, diluted in 3 ml of PBS, was injected into the tail vein over 15–20 s. All siRNAs were purchased from Applied Biosystems (Silencer^{R} In Vivo Ready Pre-designed siRNA). *Sepp1* siRNAs with the following

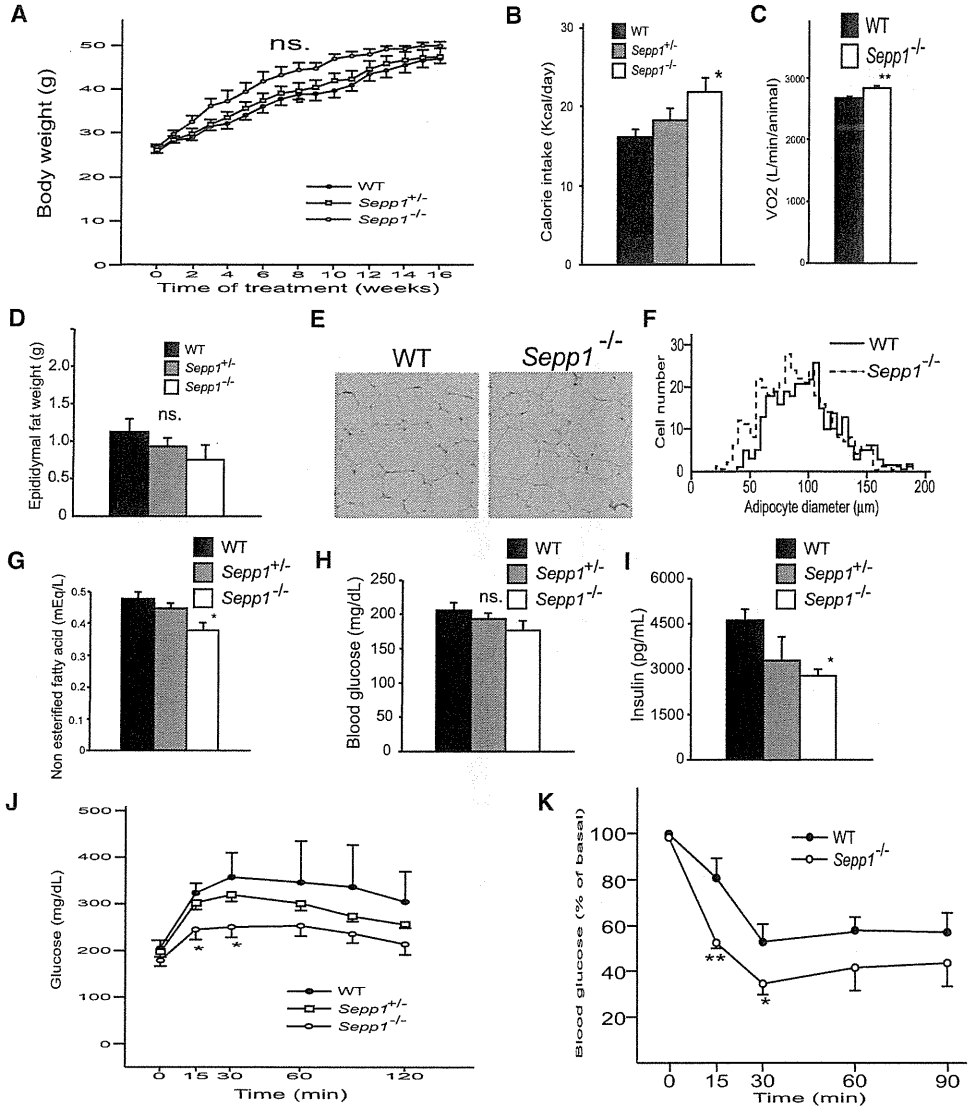

Figure 6. *Sepp1*-Deficient Mice Are Protected from Diet-Induced Insulin Resistance and Adipocyte Hypertrophy

(A) Body weight of *Sepp1*-deficient and wild-type mice fed a high-fat, high-sucrose diet (HFHSD; n = 4–8). Sixteen-week-old male mice were fed a HFHSD for 16 weeks.

(B) Daily calorie intake in *Sepp1*-deficient and wild-type mice (n = 4–8).

(C) Energy expenditure (as measured by VO_2 consumption through indirect calorimetry; n = 4).

(D) Epididymal fat mass in *Sepp1*-deficient and wild-type mice fed HFHSD (n = 4–7).

(E) Hematoxylin-and-eosin-stained epididymal fat sections from wild-type and *Sepp1*$^{-/-}$ mice.

(F) Histogram showing adipocyte diameters. We determined adipocyte diameters by measuring at least 300 adipocytes randomly selected from four independent sections.

(G) Blood nonestimated fatty acid levels in *Sepp1*-deficient and wild-type mice fed HFHSD (n = 4–7).

(H) Blood glucose levels in *Sepp1*-deficient and wild-type mice fed HFHSD (n = 4–8).

(I) Blood insulin levels in *Sepp1*-deficient and wild-type mice fed HFHSD (n = 4–8). Blood samples were obtained from mice fed a HFHSD for 16 weeks after a 12 hr fast in (G)–(I).

(J) Intraperitoneal glucose tolerance tests in wild-type and *Sepp1*-deficient mice (n = 4–8). Glucose was administered at a dose of 0.3 g/kg body weight.

(K) Intraperitoneal insulin tolerance tests in wild-type and *Sepp1*-deficient mice (n = 5–10). Insulin was administered at a dose of 2.0 units/kg body weight.

Data in (A)–(D) and (G)–(K) represent the means ± SEM from four to ten mice per group. *$p < 0.05$, **$p < 0.01$ versus wild-type mice. See also Figure S4.

sequence were synthesized: mouse *Sepp1*, 5′-GGUGUCAGAACACAUC GCAtt-3′ (sense). Negative control siRNA was also used and had no significant homology with any known gene sequences in mouse, rat, or human. Glucose and insulin loading tests were performed 2–7 days after injection of mice with siRNA.

SeP Knockout Mice

SeP knockout mice were produced by homologous recombination with genomic DNA cloned from an Sv-129 P1 library, as described previously (Hill et al., 2003). As female SeP knockout mice had inconsistent phenotypes, only male mice were used in this study.

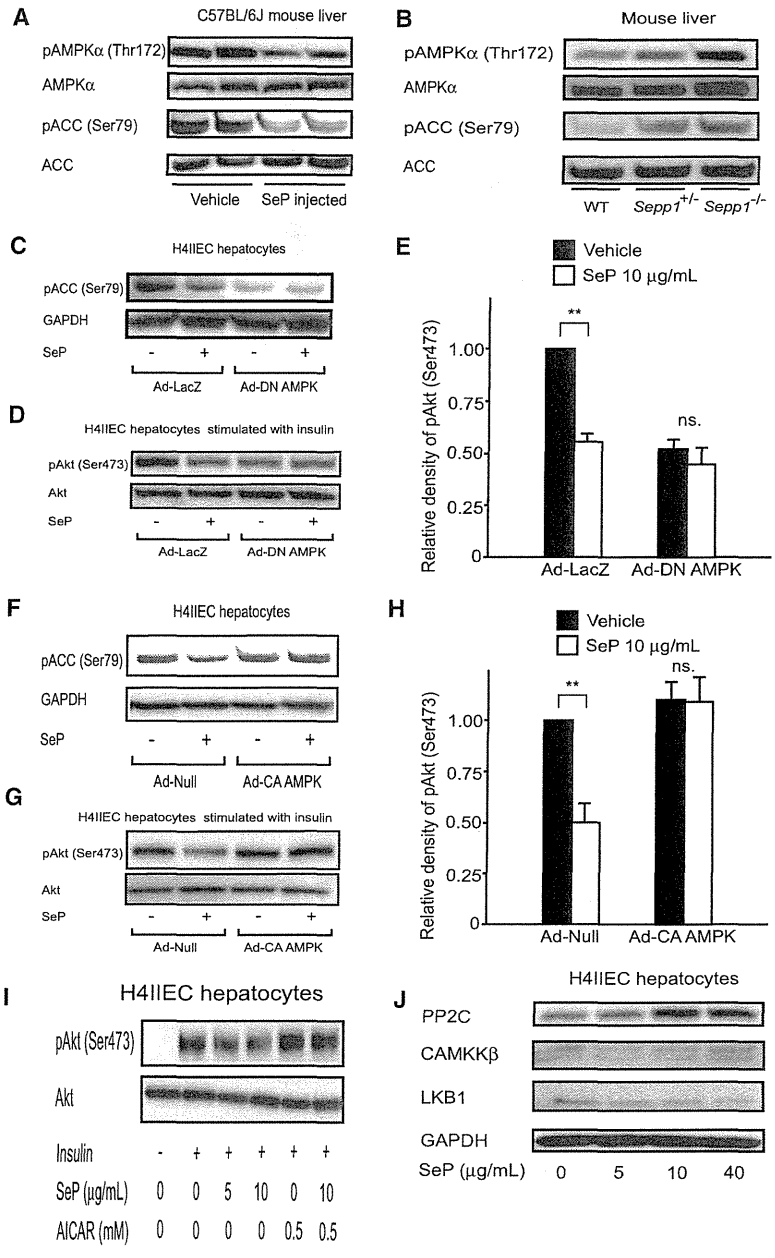

Figure 7. SeP Reduces Phosphorylation of AMPK and ACC in Hepatocytes

(A) Phosphorylation of AMPK and ACC in the liver of mice injected with SeP or vehicle. C57BL/6J mice were injected intravenously with purified human SeP (1 mg/kg body weight) or vehicle (phosphate-buffered saline). At 6 hr after injection, the liver was removed.

(B) Phosphorylation of AMPK and ACC in the liver of *Sepp1*-deficient mice after a 12 hr fast.

(C–E) Effects of dominant-negative AMPK on ACC phosphorylation (C) and insulin-stimulated Akt phosphorylation (D and E) in H4IIEC hepatocytes treated with SeP.

(F–H) Effects of constitutively active AMPK on ACC phosphorylation (F) and insulin-stimulated Akt phosphorylation (G and H) in H4IIEC hepatocytes treated with SeP.

(I) Effect of AICAR on SeP-induced insulin resistance in H4IIEC hepatocytes.

(J) Levels of PP2C, CaMKKβ, and LKB1 in H4IIEC hepatocytes treated with various concentrations of SeP for 12 hr.

Data in (E) and (H) represent the means ± SEM from three independent experiments. **p < 0.01 versus vehicle-treated cells. See also Figure S5.

Statistical Analyses

All data were analyzed using the Japanese Windows Edition of the Statistical Package for Social Science (SPSS) Version 11.0. Numeric values are reported as the mean ± SEM. Differences between two groups were assessed with unpaired two-tailed t tests. Data involving more than two groups were assessed by analysis of variance (ANOVA). Glucose and insulin tolerance tests were examined with repeated-measures ANOVA.

ACCESSION NUMBERS

Microarray data have been deposited in Gene Expression Omnibus under accession number GSE23343.

SUPPLEMENTAL INFORMATION

Supplemental Information includes Supplemental Experimental Procedures, five figures, and five tables and can be found with this article online at doi:10.1016/j.cmet.2010.09.015.

ACKNOWLEDGMENTS

We thank Kuniaki Arai of Kanazawa University for liver biopsies and Isao Usui, Hajime Ishihara, and Toshiyasu Sasaoka of Toyama University for supplying their technical expertise on Western blot analyses of phosphoproteins. We thank Yuriko Furuta and Yoko Hashimoto for technical assistance. We thank Fabienne Foufelle of Université Pierre et Marie Curie for providing adenovirus vector encoding DN-AMPK. We are indebted to Kristina E. Hill and Raymond F. Burk of Vanderbilt University School of Medicine for the *Sepp1* knockout mice. This work was supported by Takeda Science Foundation and Grants-in-Aid from the Ministry of Education, Culture, Sports, Science and Technology, Japan. We also thank Cathie Chung for editing the manuscript.

Received: February 2, 2009
Revised: April 29, 2010
Accepted: August 13, 2010
Published: November 2, 2010

REFERENCES

Andoh, A., Hirashima, M., Maeda, H., Hata, K., Inatomi, O., Tsujikawa, T., Sasaki, M., Takahashi, K., and Fujiyama, Y. (2005). Serum selenoprotein-P levels in patients with inflammatory bowel disease. Nutrition *21*, 574–579.

Auberger, P., Falquerho, L., Contreres, J.O., Pages, G., Le Cam, G., Rossi, B., and Le Cam, A. (1989). Characterization of a natural inhibitor of the insulin receptor tyrosine kinase: cDNA cloning, purification, and anti-mitogenic activity. Cell *58*, 631–640.

Bellinger, F.P., He, Q.P., Bellinger, M.T., Lin, Y., Raman, A.V., White, L.R., and Berry, M.J. (2008). Association of selenoprotein p with Alzheimer's pathology in human cortex. J. Alzheimers Dis. *15*, 465–472.

Bleys, J., Navas-Acien, A., and Guallar, E. (2007). Serum selenium and diabetes in U.S. adults. Diabetes Care *30*, 829–834.

Burk, R.F., and Hill, K.E. (2005). Selenoprotein P: an extracellular protein with unique physical characteristics and a role in selenium homeostasis. Annu. Rev. Nutr. *25*, 215–235.

Burk, R.F., Hill, K.E., Olson, G.E., Weeber, E.J., Motley, A.K., Winfrey, V.P., and Austin, L.M. (2007). Deletion of apolipoprotein E receptor-2 in mice lowers brain selenium and causes severe neurological dysfunction and death when a low-selenium diet is fed. J. Neurosci. *27*, 6207–6211.

Carlson, B.A., Novoselov, S.V., Kumaraswamy, E., Lee, B.J., Anver, M.R., Gladyshev, V.N., and Hatfield, D.L. (2004). Specific excision of the selenocysteine tRNA[Ser]Sec (Trsp) gene in mouse liver demonstrates an essential role of selenoproteins in liver function. J. Biol. Chem. *279*, 8011–8017.

Davies, S.P., Helps, N.R., Cohen, P.T., and Hardie, D.G. (1995). 5′-AMP inhibits dephosphorylation, as well as promoting phosphorylation, of the AMP-activated protein kinase. Studies using bacterially expressed human protein phosphatase-2C alpha and native bovine protein phosphatase-2AC. FEBS Lett. *377*, 421–425.

Després, J.P., Lamarche, B., Mauriège, P., Cantin, B., Dagenais, G.R., Moorjani, S., and Lupien, P.J. (1996). Hyperinsulinemia as an independent risk factor for ischemic heart disease. N. Engl. J. Med. *334*, 952–957.

Friedman, J.M., and Halaas, J.L. (1998). Leptin and the regulation of body weight in mammals. Nature *395*, 763–770.

Hill, K.E., Zhou, J., McMahan, W.J., Motley, A.K., Atkins, J.F., Gesteland, R.F., and Burk, R.F. (2003). Deletion of selenoprotein P alters distribution of selenium in the mouse. J. Biol. Chem. *278*, 13640–13646.

Kahn, B.B., Alquier, T., Carling, D., and Hardie, D.G. (2005). AMP-activated protein kinase: ancient energy gauge provides clues to modern understanding of metabolism. Cell Metab. *1*, 15–25.

Kawano, K., Hirashima, T., Mori, S., Saitoh, Y., Kurosumi, M., and Natori, T. (1992). Spontaneous long-term hyperglycemic rat with diabetic complications. Otsuka Long-Evans Tokushima Fatty (OLETF) strain. Diabetes *41*, 1422–1428.

Maeda, K., Okubo, K., Shimomura, I., Funahashi, T., Matsuzawa, Y., and Matsubara, K. (1996). cDNA cloning and expression of a novel adipose specific collagen-like factor, apM1 (AdiPose Most abundant Gene transcript 1). Biochem. Biophys. Res. Commun. *221*, 286–289.

Maeda, N., Shimomura, I., Kishida, K., Nishizawa, H., Matsuda, M., Nagaretani, H., Furuyama, N., Kondo, H., Takahashi, M., Arita, Y., et al. (2002). Diet-induced insulin resistance in mice lacking adiponectin/ACRP30. Nat. Med. *8*, 731–737.

Masiulis, I., Quill, T.A., Burk, R.F., and Herz, J. (2009). Differential functions of the Apoer2 intracellular domain in selenium uptake and cell signaling. Biol. Chem. *390*, 67–73.

McCaffrey, A.P., Meuse, L., Pham, T.T., Conklin, D.S., Hannon, G.J., and Kay, M.A. (2002). RNA interference in adult mice. Nature *418*, 38–39.

Minokoshi, Y., Kim, Y.B., Peroni, O.D., Fryer, L.G., Müller, C., Carling, D., and Kahn, B.B. (2002). Leptin stimulates fatty-acid oxidation by activating AMP-activated protein kinase. Nature *415*, 339–343.

Misu, H., Takamura, T., Matsuzawa, N., Shimizu, A., Ota, T., Sakurai, M., Ando, H., Arai, K., Yamashita, T., Honda, M., et al. (2007). Genes involved in oxidative phosphorylation are coordinately upregulated with fasting hyperglycaemia in livers of patients with type 2 diabetes. Diabetologia *50*, 268–277.

Oike, Y., Akao, M., Yasunaga, K., Yamauchi, T., Morisada, T., Ito, Y., Urano, T., Kimura, Y., Kubota, Y., Maekawa, H., et al. (2005). Angiopoietin-related growth factor antagonizes obesity and insulin resistance. Nat. Med. *11*, 400–408.

Olson, G.E., Winfrey, V.P., Nagdas, S.K., Hill, K.E., and Burk, R.F. (2007). Apolipoprotein E receptor-2 (ApoER2) mediates selenium uptake from selenoprotein P by the mouse testis. J. Biol. Chem. *282*, 12290–12297.

Ota, T., Takamura, T., Kurita, S., Matsuzawa, N., Kita, Y., Uno, M., Akahori, H., Misu, H., Sakurai, M., Zen, Y., et al. (2007). Insulin resistance accelerates a dietary rat model of nonalcoholic steatohepatitis. Gastroenterology *132*, 282–293.

Persson-Moschos, M., Alfthan, G., and Akesson, B. (1998). Plasma selenoprotein P levels of healthy males in different selenium status after oral supplementation with different forms of selenium. Eur. J. Clin. Nutr. *52*, 363–367.

Saito, Y., and Takahashi, K. (2002). Characterization of selenoprotein P as a selenium supply protein. Eur. J. Biochem. *269*, 5746–5751.

Saito, Y., Hayashi, T., Tanaka, A., Watanabe, Y., Suzuki, M., Saito, E., and Takahashi, K. (1999). Selenoprotein P in human plasma as an extracellular phospholipid hydroperoxide glutathione peroxidase. Isolation and enzymatic characterization of human selenoprotein p. J. Biol. Chem. *274*, 2866–2871.

Saito, Y., Watanabe, Y., Saito, E., Honjoh, T., and Takahashi, K. (2001). Production and application of monoclonal antibodies to human selenoprotein P. J. Health Sci. *47*, 346–352.

Saltiel, A.R., and Kahn, C.R. (2001). Insulin signalling and the regulation of glucose and lipid metabolism. Nature *414*, 799–806.

Scherer, P.E., Williams, S., Fogliano, M., Baldini, G., and Lodish, H.F. (1995). A novel serum protein similar to C1q, produced exclusively in adipocytes. J. Biol. Chem. *270*, 26746–26749.

Schomburg, L., Schweizer, U., Holtmann, B., Flohé, L., Sendtner, M., and Köhrle, J. (2003). Gene disruption discloses role of selenoprotein P in selenium delivery to target tissues. Biochem. J. *370*, 397–402.

Speckmann, B., Walter, P.L., Alili, L., Reinehr, R., Sies, H., Klotz, L.O., and Steinbrenner, H. (2008). Selenoprotein P expression is controlled through interaction of the coactivator PGC-1alpha with FoxO1a and hepatocyte nuclear factor 4alpha transcription factors. Hepatology *48*, 1998–2006.

Srinivas, P.R., Wagner, A.S., Reddy, L.V., Deutsch, D.D., Leon, M.A., Goustin, A.S., and Grunberger, G. (1993). Serum alpha 2-HS-glycoprotein is an inhibitor of the human insulin receptor at the tyrosine kinase level. Mol. Endocrinol. *7*, 1445–1455.

Steinberg, G.R., Michell, B.J., van Denderen, B.J., Watt, M.J., Carey, A.L., Fam, B.C., Andrikopoulos, S., Proietto, J., Görgün, C.Z., Carling, D., et al. (2006). Tumor necrosis factor alpha-induced skeletal muscle insulin resistance involves suppression of AMP-kinase signaling. Cell Metab. *4*, 465–474.

Steppan, C.M., Bailey, S.T., Bhat, S., Brown, E.J., Banerjee, R.R., Wright, C.M., Patel, H.R., Ahima, R.S., and Lazar, M.A. (2001). The hormone resistin links obesity to diabetes. Nature *409*, 307–312.

Takamura, T., Sakurai, M., Ota, T., Ando, H., Honda, M., and Kaneko, S. (2004). Genes for systemic vascular complications are differentially expressed in the livers of type 2 diabetic patients. Diabetologia *47*, 638–647.

Takeda, S., Sato, N., Uchio-Yamada, K., Sawada, K., Kunieda, T., Takeuchi, D., Kurinami, H., Shinohara, M., Rakugi, H., and Morishita, R. (2010). Diabetes-accelerated memory dysfunction via cerebrovascular inflammation and Abeta deposition in an Alzheimer mouse model with diabetes. Proc. Natl. Acad. Sci. USA *107*, 7036–7041.

Takeshita, Y., Takamura, T., Hamaguchi, E., Shimizu, A., Ota, T., Sakurai, M., and Kaneko, S. (2006). Tumor necrosis factor-alpha-induced production of plasminogen activator inhibitor 1 and its regulation by pioglitazone and cerivastatin in a nonmalignant human hepatocyte cell line. Metabolism *55*, 1464–1472.

Velculescu, V.E., Zhang, L., Vogelstein, B., and Kinzler, K.W. (1995). Serial analysis of gene expression. Science *270*, 484–487.

Walter, P.L., Steinbrenner, H., Barthel, A., and Klotz, L.O. (2008). Stimulation of selenoprotein P promoter activity in hepatoma cells by FoxO1a transcription factor. Biochem. Biophys. Res. Commun. *365*, 316–321.

Xu, A., Lam, M.C., Chan, K.W., Wang, Y., Zhang, J., Hoo, R.L., Xu, J.Y., Chen, B., Chow, W.S., Tso, A.W., and Lam, K.S. (2005). Angiopoietin-like protein 4 decreases blood glucose and improves glucose tolerance but induces hyperlipidemia and hepatic steatosis in mice. Proc. Natl. Acad. Sci. USA *102*, 6086–6091.

Yamauchi, T., Kamon, J., Minokoshi, Y., Ito, Y., Waki, H., Uchida, S., Yamashita, S., Noda, M., Kita, S., Ueki, K., et al. (2002). Adiponectin stimulates glucose utilization and fatty-acid oxidation by activating AMP-activated protein kinase. Nat. Med. *8*, 1288–1295.

Yang, Q., Graham, T.E., Mody, N., Preitner, F., Peroni, O.D., Zabolotny, J.M., Kotani, K., Quadro, L., and Kahn, B.B. (2005). Serum retinol binding protein 4 contributes to insulin resistance in obesity and type 2 diabetes. Nature *436*, 356–362.

Zender, L., Hutker, S., Liedtke, C., Tillmann, H.L., Zender, S., Mundt, B., Waltemathe, M., Gosling, T., Flemming, P., Malek, N.P., et al. (2003). Caspase 8 small interfering RNA prevents acute liver failure in mice. Proc. Natl. Acad. Sci. USA *100*, 7797–7802.

Cell Metabolism
Article

Impaired Insulin Signaling in Endothelial Cells Reduces Insulin-Induced Glucose Uptake by Skeletal Muscle

Tetsuya Kubota,[1,3,5,18] Naoto Kubota,[1,3,6,18,*] Hiroki Kumagai,[1,18] Shinichi Yamaguchi,[1] Hideki Kozono,[1] Takehiro Takahashi,[1] Mariko Inoue,[1,3] Shinsuke Itoh,[1] Iseki Takamoto,[1,6] Takayoshi Sasako,[1] Katsuyoshi Kumagai,[1,6] Tomoko Kawai,[1,3] Shinji Hashimoto,[1] Tsuneo Kobayashi,[7] Maki Sato,[8] Kumpei Tokuyama,[8] Satoshi Nishimura,[2] Masaki Tsunoda,[9] Tomohiro Ide,[9] Koji Murakami,[9] Tomomi Yamazaki,[4] Osamu Ezaki,[4] Koichi Kawamura,[10] Hirotake Masuda,[10] Masao Moroi,[5] Kaoru Sugi,[5] Yuichi Oike,[11] Hiroaki Shimokawa,[12] Nobuyuki Yanagihara,[13] Masato Tsutsui,[14] Yasuo Terauchi,[15] Kazuyuki Tobe,[16] Ryozo Nagai,[2,6] Katsuo Kamata,[7] Kenji Inoue,[17] Tatsuhiko Kodama,[6,17] Kohjiro Ueki,[1,6] and Takashi Kadowaki[1,3,6,*]

[1]Department of Diabetes and Metabolic Diseases
[2]Department of Cardiovascular Diseases
Graduate School of Medicine, University of Tokyo, Tokyo 113-8655, Japan
[3]Clinical Nutrition Program
[4]Nutritional Science Program
National Institute of Health and Nutrition, Tokyo 162-8636, Japan
[5]Division of Cardiovascular Medicine, Toho University Ohashi Medical Center, Tokyo 113-8655, Japan
[6]Translational Systems Biology and Medicine Initiative, University of Tokyo, Tokyo 153-8515, Japan
[7]Department of Physiology and Morphology, Institute of Medicinal Chemistry, Hoshi University, Tokyo 142-8501, Japan
[8]Graduate School of Comprehensive Human Science, University of Tsukuba, Tsukuba 305-8577, Japan
[9]Bioscience Division 1, Metabolic Discovery Research Laboratories, Kyorin Pharmaceutical Co. Ltd., Shimotsuga 329-0014, Japan
[10]Second Department of Pathology, Akita University School of Medicine, Akita 010-8543, Japan
[11]Department of Molecular Genetics, Graduate School of Medical Sciences, Kumamoto University, Kumamoto 860-8556, Japan
[12]Department of Cardiovascular Medicine, Tohoku University Graduate School of Medicine, Sendai 980-8574, Japan
[13]Department of Pharmacology, University of Occupational and Environmental Health, School of Medicine, Kitakyushu 807-8555, Japan
[14]Department of Pharmacology, Faculty of Medicine, University of the Ryukyu, Okinawa 903-0215, Japan
[15]Department of Diabetes and Endocrinology, Yokohama City University, School of Medicine, Kanagawa 236-0004, Japan
[16]First Department of Internal Medicine, Faculty of Medicine, University of Toyama, Toyama, 930-0194, Japan
[17]Laboratory for Systems Biology and Medicine, Research Center for Advanced Science and Technology, University of Tokyo, Tokyo 153-8904, Japan
[18]These authors contributed equally to this work
*Correspondence: kadowaki-3im@h.u-tokyo.ac.jp (T.K.), nkubota-tky@umin.ac.jp (N.K.)
DOI 10.1016/j.cmet.2011.01.018

SUMMARY

In obese patients with type 2 diabetes, insulin delivery to and insulin-dependent glucose uptake by skeletal muscle are delayed and impaired. The mechanisms underlying the delay and impairment are unclear. We demonstrate that impaired insulin signaling in endothelial cells, due to reduced Irs2 expression and insulin-induced eNOS phosphorylation, causes attenuation of insulin-induced capillary recruitment and insulin delivery, which in turn reduces glucose uptake by skeletal muscle. Moreover, restoration of insulin-induced eNOS phosphorylation in endothelial cells completely reverses the reduction in capillary recruitment and insulin delivery in tissue-specific knockout mice lacking Irs2 in endothelial cells and fed a high-fat diet. As a result, glucose uptake by skeletal muscle is restored in these mice. Taken together, our results show that insulin signaling in endothelial cells plays a pivotal role in the regulation of glucose uptake by skeletal muscle. Furthermore, improving endothelial insulin signaling may serve as a therapeutic strategy for ameliorating skeletal muscle insulin resistance.

INTRODUCTION

Skeletal muscle is one of the major target organs of insulin actions and plays an essential role in insulin-induced glucose uptake (DeFronzo et al., 1979; Bergman, 1989). Insulin, secreted by the pancreatic β cells, is delivered into the capillaries and crosses the endothelial barrier to enter the interstitial spaces (Vincent et al., 2005). It then binds to the insulin receptors on the skeletal muscle cell surface, activating intracellular pathways in the skeletal muscle (White and Kahn, 1994; Petersen et al., 2004; Long and Zierath, 2008). Recent evidence indicates that insulin delivery to the skeletal muscle interstitium is the rate-limiting step in insulin-stimulated glucose uptake by the skeletal muscle, and is much slower in obese insulin-resistant subjects than in normal subjects (Sherwin et al., 1974; DeFronzo et al., 1979; Yang et al., 1989; Jansson et al., 1993; Miles et al., 1995; Sjostrand et al., 2002; Barrett et al., 2009). Andres and colleagues have shown that insulin is distributed more slowly

to the compartment corresponding to the skeletal muscle than to other compartments, and the time course of insulin equilibration with this pool closely paralleled the glucose infusion rate (GIR) in their compartmental model (Sherwin et al., 1974; DeFronzo et al., 1979). Moreover, the dynamics of insulin concentrations in the skeletal muscle lymphatics, which is derived from the interstitial fluid in the skeletal muscle, is actually slow, and is significantly correlated with the peripheral glucose uptake after insulin infusion (Yang et al., 1989). In obese subjects, the appearance of insulin in the interstitial fluid of the skeletal muscle and onset of insulin action after insulin infusion were found to be significantly delayed in comparison with the results in control subjects (Sjostrand et al., 2002). Although the slow onset of insulin action on glucose disposal in vivo could be secondary to a slow response by the cellular machinery within the myocytes, which are the cells responsible for glucose uptake in the skeletal muscle, insulin-induced glucose uptake by myocytes in vitro appears to be fully activated within 2–5 min, much earlier than that in vivo (Karnieli et al., 1981). Moreover, Bergman et al. demonstrated that injection of insulin directly into the interstitium of the skeletal muscle is followed by a prompt increase in the glucose uptake (Chiu et al., 2008). Based on these findings, insulin delivery may determine the in vivo time course of insulin-induced glucose uptake, which may be much slower than the insulin-induced glucose uptake in vitro.

Two discrete steps have been reported to increase insulin delivery to the skeletal muscle: an increase in the available capillary surface area (capillary recruitment), and an increase in the transendothelial transport of insulin. Clark and colleagues measured capillary recruitment following insulin infusion and found that it was associated with increased glucose uptake by the skeletal muscle (Rattigan et al., 1997; Vincent et al., 2004). The insulin-induced capillary recruitment and glucose uptake were reported to be significantly impaired in obese subjects and diabetic models (Wallis et al., 2002; Keske et al., 2009). In addition to the vasoactive actions of insulin on the capillaries, insulin may promote its own movement across the endothelial barrier. Recent in vivo evidence suggests that transendothelial transport of insulin in the skeletal muscle increased along with elevation of the plasma insulin levels, and that these levels were diminished in the presence of high-fat (HF) diet-induced insulin resistance (Hamilton-Wessler et al., 2002; Ellmerer et al., 2006; Wang et al., 2008). It is still unclear whether capillary recruitment and transendothelial transport of insulin may be related or may function independently (Clark, 2008).

We hypothesized that an insulin signaling defect in the endothelial cells impairs insulin-induced capillary recruitment and insulin delivery in the skeletal muscle in obesity. In HF diet-fed obese mice, the expression levels of insulin receptor substrate (Irs)2, which is the major Irs isoform expressed in the endothelial cells (Kubota et al., 2003), were markedly reduced, and insulin-induced eNOS phosphorylation, capillary recruitment, and insulin delivery were markedly impaired. Consistent with these results, mice with Irs2 deletion in the endothelial cells (ETIrs2KO mice) also exhibited a reduction of insulin-induced eNOS phosphorylation, capillary recruitment, and insulin delivery. Moreover, restoration of the insulin-induced eNOS phosphorylation in the endothelial cells completely reversed the reduction of the capillary recruitment and insulin delivery in both the HF diet-fed and ETIrs2KO mice. We conclude that a genetically and/or environmentally induced insulin signaling defect in the endothelial cells causes skeletal muscle insulin resistance as a consequence of the impaired insulin-induced capillary recruitment and insulin delivery.

RESULTS

Insulin Signaling Was Significantly Impaired in the Endothelial Cells of the ob/ob and HF Diet-Fed Mice

To investigate insulin signaling in the endothelial cells in mouse models of obesity, we first measured the expression levels of the insulin receptor (Ir) and Ir substrate (Irs) in mice with genetically (ob/ob mice) or environmentally induced (8-week HF diet-fed mice) obesity. Although there were no significant differences in the mRNA or protein expression levels of Ir and endothelin (ET)-1 (see Figures S1A and S1B available online), the mRNA and protein expression levels of Irs1 were reduced by approximately 50% and those of Irs2, the major Irs isoform expressed on the endothelial cells (Kubota et al., 2003), by approximately 80% in the endothelial cells of both the mouse models of obesity (Figures 1A and 1B). To elucidate the mechanisms by which the expressions of Irs1 and Irs2 in the endothelial cells were downregulated, we investigated the effects of FFA on the expressions of Irs1 and Irs2 following continuous administration of intralipid for 24 hr in C57Bl/6 mice. Although a 7-fold increase of the plasma FFA levels was observed after the intralipid treatment, the expression levels of Irs1 and Irs2 measured before and after the intralipid treatment were not significantly different (Figure S1C). We next investigated whether the Irs1 and Irs2 gene expressions in the endothelial cells might be altered by hyperinsulinemia induced by continuous administration of insulin for 24 hr using a miniosmotic pump in C57Bl/6 mice. After continuous administration of insulin for 24 hr, a 7-fold increase of the plasma insulin levels was noted (Figure 1C). In regard to the expression levels of the Irs1 and Irs2, on the other hand, while no change in the expression of endothelial Irs1 was observed, the expression of endothelial Irs2 was significantly decreased (Figure 1C). These data suggest that hyperinsulinemia may be one of the mechanisms underlying the decrease in the expression of endothelial Irs2 observed in the ob/ob and HF diet-fed mice, although the reason for the downregulated Irs1 expression in these mice still remains unexplained. The insulin signaling cascade activates Akt, which in turn phosphorylates and activates eNOS in the endothelial cells (Muniyappa and Quon, 2007). Consistent with the results for the expression levels of Irs1 and Irs2, insulin-stimulated phosphorylations of Akt and eNOS were decreased by 70%–80% in the endothelial cells of the ob/ob and HF diet-fed mice (Figure 1D), indicating that insulin signaling was impaired in the endothelial cells of these obesity models. We then investigated whether impaired insulin signaling in the endothelial cells might be involved in the HF diet-induced, obesity-linked impairment of glucose uptake by the skeletal muscle. Although an increase of the capillary blood volume at 10 min after the insulin infusion in the hyperinsulinemic-euglycemic clamp study was observed in the normal chow-fed mice, no such increase was observed in the HF diet-fed mice (Figure 1E). On the other hand, no increase of

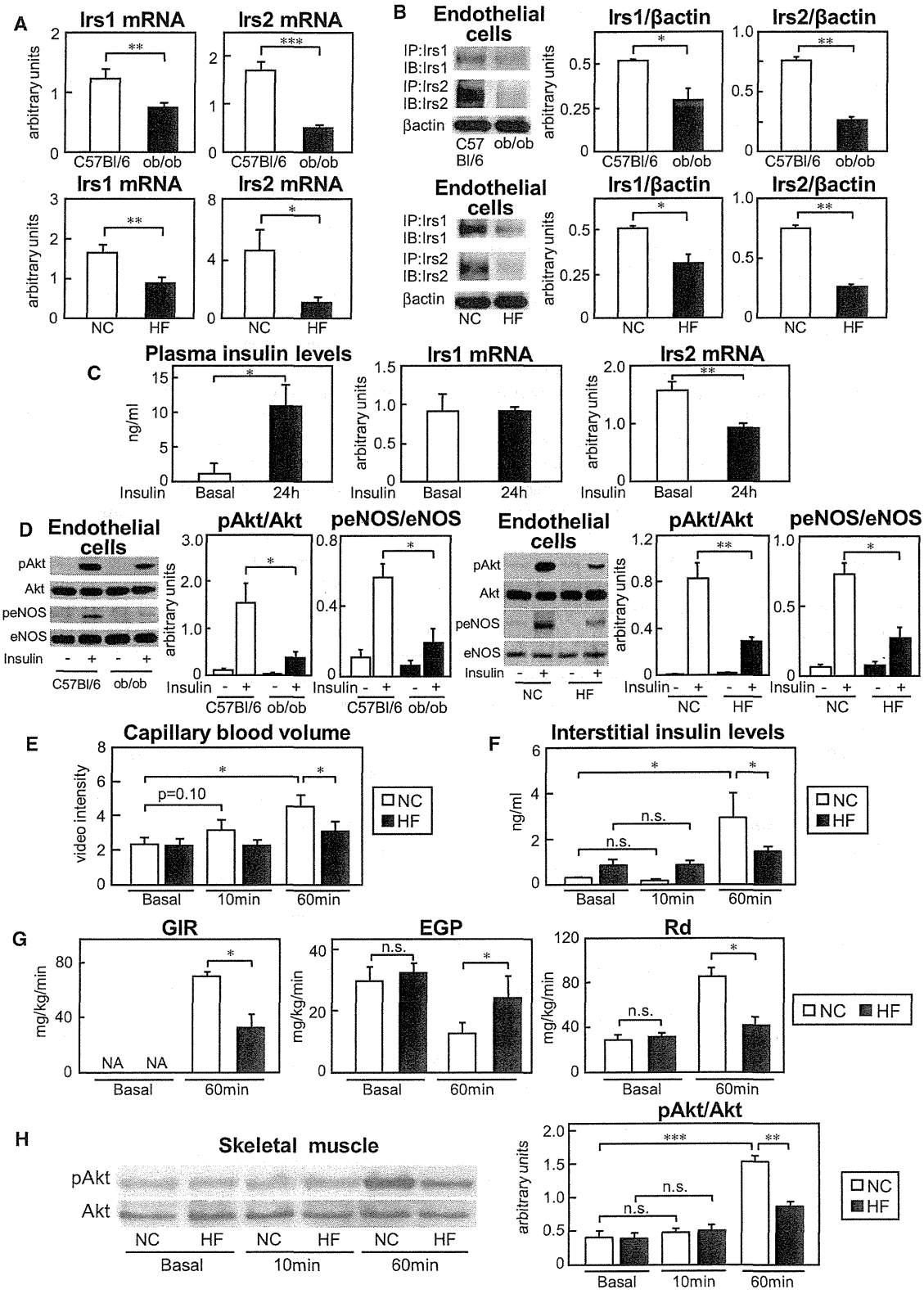

Figure 1. In the HF Diet-Fed Obese Mice, which Show Impaired Glucose Uptake by the Skeletal Muscle, Decreased Insulin-Induced Phosphorylation of eNOS in the Endothelial Cells, along with Downregulation, Mainly of Irs2, Was Associated with Attenuation of the Insulin-Induced Increase of the Capillary Blood Volume and of the Increase of the Interstitial Concentrations of Insulin

(A and B) Expression levels of Irs1 or Irs2 mRNA and protein in the endothelial cells of the ob/ob and HF diet-fed mice (n = 3–11).

the interstitial concentrations of insulin was observed at 10 min after the insulin infusion in either the normal chow-fed or the HF diet-fed mice (Figure 1F). These data suggest that capillary recruitment starts to increase well before the increase of the interstitial insulin concentrations, consistent with the results of previous studies (Miles et al., 1995; Vincent et al., 2005). Insulin-induced increases of the capillary blood volume and interstitial concentrations of insulin were significantly impaired at 60 and 120 min after the insulin infusion in the hyperinsulinemic-euglycemic clamp study (Figures 1E and 1F; Movies S1A and S1B, and data not shown), even when the plasma insulin levels were adjusted to be the same in both the normal chow-fed and HF diet-fed mice (Figure S1D and data not shown). A significant decrease of the GIR and glucose disappearance rate (Rd), as also a significant increase of the endogenous glucose production (EGP), were found in the animals at 60 and 120 min after the insulin infusion in the hyperinsulinemic-euglycemic clamp study (Figure 1G and data not shown). Consistent with these results, the phosphorylation levels of Akt in the skeletal muscle in the normal chow-fed mice began to increase by 30 min and reached its peak about 60 min after the insulin infusion, whereas this increase of the Akt phosphorylation level from 30 min onward after the insulin infusion in the hyperinsulinemic-euglycemic clamp study was significantly impaired in the HF diet-fed mice (Figure 1H; Figure S1E and data not shown). These data suggest that the decreased phosphorylation level of eNOS induced by insulin in the endothelial cells associated with downregulation, mainly of Irs2, appears to be involved, along with the impaired insulin-induced capillary recruitment and increase of the interstitial concentrations of insulin, in the impaired glucose uptake by the skeletal muscle in the HF diet-fed obese mice.

ETIrs2KO Mice Exhibited Impaired Insulin-Induced Glucose Uptake by the Skeletal Muscle

In order to elucidate the causal relationship between insulin signaling in the endothelial cells and the glucose uptake by the skeletal muscle, we generated ETIrs2KO mice. The endothelial Irs2 mRNA levels were reduced by approximately 95% in the ETIrs2KO mice, whereas the Irs2 expression levels in the white adipose tissue (WAT), liver, and skeletal muscle remained unchanged (Figures 2A and 2B). The Irs2 protein expression and insulin-stimulated tyrosine phosphorylation of Irs2 were almost completely abrogated in the endothelial cells of the ETIrs2KO mice (Figure 2C). There were no significant differences in the mRNA and protein levels of eNOS or ET-1 between the control and ETIrs2KO mice (Figures S2A and S2B). The basal blood glucose and plasma insulin levels were indistinguishable between the control and ETIrs2KO mice (Figure S2C). Insulin-stimulated phosphorylations of Akt and eNOS were found to be significantly reduced in the endothelial cells of the ETIrs2KO mice (Figure 2D). Although an increase of the capillary blood volume was observed in the control mice by 10 min after the insulin infusion in the hyperinsulinemic-euglycemic clamp study, no such increase was observed in the ETIrs2KO mice (Figure 2E). In contrast, no increase in the interstitial concentrations of insulin was observed at 10 min after the insulin infusion in either the control or the ETIrs2KO mice (Figure 2F). The insulin-induced increases of the capillary blood volume and interstitial concentrations of insulin were significantly impaired at 60 and 120 min after insulin infusion in the hyperinsulinemic-euglycemic clamp study (Figures 2E and 2F and data not shown), even when the plasma insulin levels were adjusted to be the same in both the control and ETIrs2KO mice (Figure S2D and data not shown). Furthermore, the whole-body insulin sensitivity and glucose tolerance were also significantly impaired in the ETIrs2KO mice (Figures 2G and 2H). The GIR and Rd at 60 and 120 min after insulin infusion in the hyperinsulinemic-euglycemic clamp study were significantly reduced in the ETIrs2KO mice (Figure 2I and data not shown). The decreased Rd observed in the ETIrs2KO mice during the hyperinsulinemic-euglycemic clamp, however, indicates impairment of glucose uptake by mainly the skeletal muscle, but also by other tissues containing nonfenestrated endothelial cells forming tight junctions. Thus, we also measured the insulin-induced glucose uptake by the skeletal muscle during the hyperinsulinemic-euglycemic clamp study using 2-deoxy-[^{3}H]glucose (2-[^{3}H]DG). Consistent with the results obtained for the Rd, the skeletal muscle glucose uptake was significantly reduced in the ETIrs2KO mice (Figure 2J), suggesting that the glucose uptake through the capillaries, at least, was impaired in the skeletal muscle of the ETIrs2KO mice. In contrast, glucose uptake by the isolated skeletal muscle from the ETIrs2KO mice was not impaired (Figure 2K), indicating that glucose uptake by the skeletal muscle per se was not impaired in the ETIrs2KO mice. Consistent with these results, the phosphorylation level of Akt in the skeletal muscle in the control mice began to increase by 30 min and reached its peak about 60 min after insulin infusion in the hyperinsulinemic-euglycemic clamp study, whereas this increase in the Akt phosphorylation level was significantly impaired in the ETIrs2KO mice (Figure 2L; Figure S2E and data not shown). Moreover, the phosphorylation levels of Irβ, as well as those of Irs1 and Akt, in the skeletal muscle were also significantly decreased in the ETIrs2KO mice at 60 min after insulin infusion into the inferior vena cava (Figure S2F). In contrast, no significant differences in the phosphorylation levels of Irβ, Irs1, Irs2, or Akt in the liver were observed between the control and ETIrs2KO mice (Figure S2G), even though Irs2 was also deleted from the hepatic endothelial cells of the ETIrs2KO mice (Figure S2H). Quantitative analysis revealed no significant difference in the β cell mass between the control and ETIrs2KO mice (Figure S2I). These data suggest that Irs2 deletion in the endothelial cells causes an insulin

(C) Expression levels of Irs1 and Irs2 mRNA after insulin infusion (n = 3–4).
(D) Phosphorylation levels of Akt and eNOS in the ob/ob and HF diet-fed mice (n = 4–7).
(E and F) Capillary blood volume (E) and interstitial insulin levels (F) in the HF diet-fed mice (n = 3–10).
(G) GIR, EGP, and Rd in the HF diet-fed mice after insulin infusion in the hyperinsulinemic-euglycemic clamp study (n = 7–9).
(H) Phosphorylation levels of Akt (ser473) in the skeletal muscle of the HF diet-fed mice after insulin infusion in the hyperinsulinemic-euglycemic clamp study (n = 3–4). "NC" indicates normal chow-fed mice. "NA" indicates not applicable. Where error bars are shown, the results represent the means ± SEM. *$p < 0.05$, **$p < 0.01$, ***$p < 0.001$.

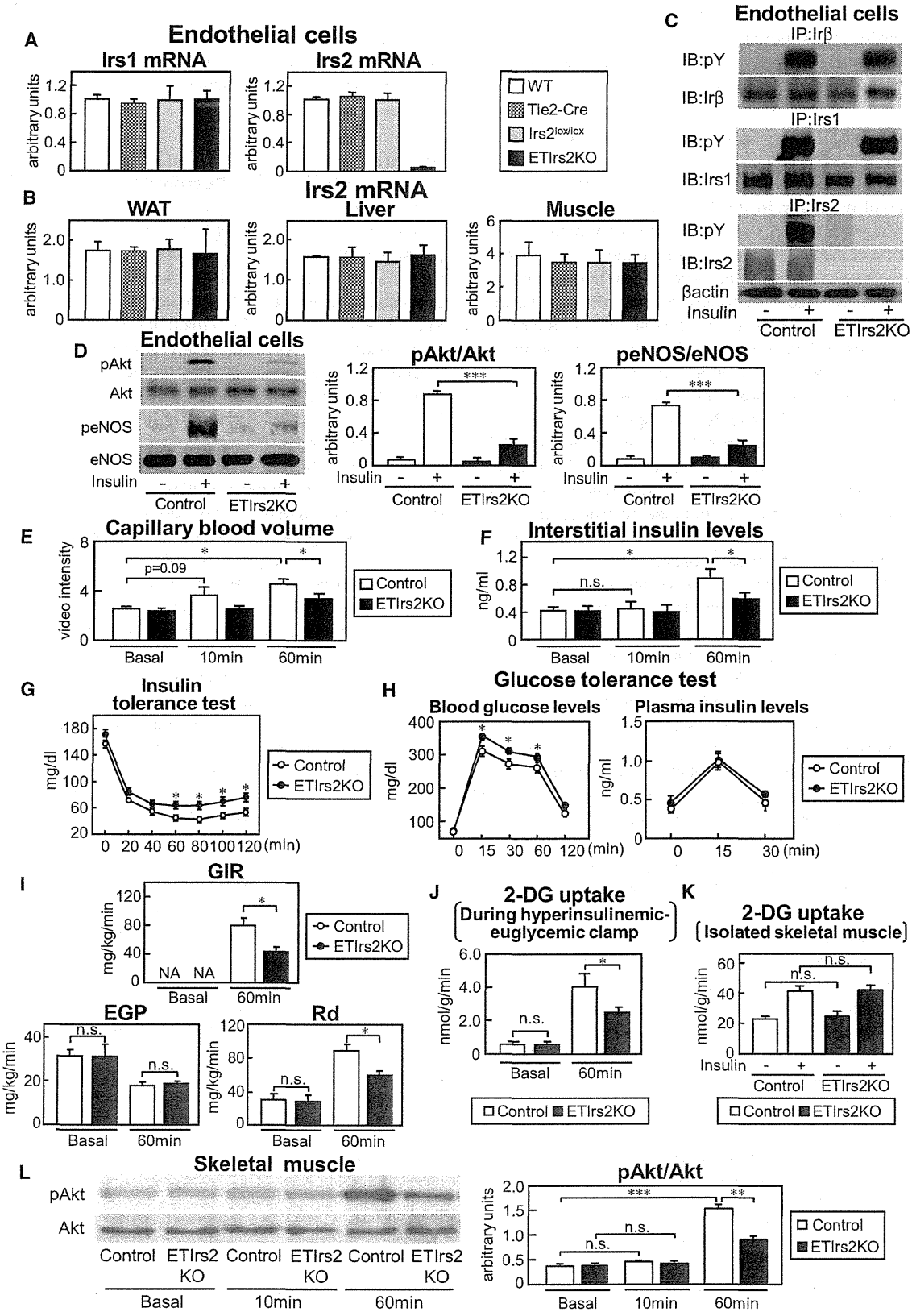
A
Endothelial cells
Irs1 mRNA
Irs2 mRNA
arbitrary units
WT
Tie2-Cre
Irs2lox/lox
ETIrs2KO
B
Irs2 mRNA
WAT
Liver
Muscle
C
Endothelial cells
IP:Irβ
IB:pY
IB:Irβ
IP:Irs1
IB:Irs1
IP:Irs2
IB:Irs2
βactin
Insulin
Control
ETIrs2KO
D
Endothelial cells
pAkt
Akt
peNOS
eNOS
pAkt/Akt
peNOS/eNOS
E
Capillary blood volume
video intensity
p=0.09
Basal
10min
60min
F
Interstitial insulin levels
ng/ml
n.s.
G
Insulin tolerance test
mg/dl
(min)
H
Glucose tolerance test
Blood glucose levels
Plasma insulin levels
I
GIR
mg/kg/min
NA
EGP
Rd
J
2-DG uptake
(During hyperinsulinemic-euglycemic clamp)
nmol/g/min
K
2-DG uptake
(Isolated skeletal muscle)
L
Skeletal muscle
pAkt
Akt
Control
ETIrs2 KO
Basal
10min
60min

signaling defect in the cells that results in impairment of insulin-induced eNOS phosphorylation, capillary recruitment, and increase of the interstitial concentrations of insulin, consequently impairing the skeletal muscle glucose uptake.

Insulin-Induced Glucose Uptake by the Skeletal Muscle Was Not Impaired in the ETIrs1KO Mice, but Was Significantly Reduced in the ETIrs1/2DKO Mice, as Compared with that in the ETIrs2KO Mice

To investigate the role of Irs1 expressed in the endothelial cells in the regulation of insulin-induced glucose uptake by the skeletal muscle, we generated mice with endothelial-cell-specific Irs1 knockout (ETIrs1KO mice). Although the Irs1 mRNA and protein levels were almost completely abrogated in the endothelial cells of the ETIrs1KO mice (Figures 3A and 3B), no significant differences in the expression levels of Irs2, eNOS, or ET-1 mRNA and protein were observed between the control and ETIrs1KO mice (Figures 3A and 3B). No significant difference in the insulin-stimulated phosphorylation levels of Akt or eNOS was observed between the control and ETIrs1KO mice (Figure 3C). Furthermore, no significant differences in the results of the insulin tolerance test or glucose tolerance test were observed between the control and ETIrs1KO mice (Figures 3D and 3E). Consistent with these results, there were also no significant differences in the results of the hyperinsulinemic-euglycemic clamp study between the control and ETIrs1KO mice (Figure 3F).

We next generated mice with endothelial-cell-specific Irs1/Irs2 double-knockout (ETIrs1/2DKO), in an attempt to elucidate whether insulin signaling in the endothelial cells might be exclusively mediated by Irs1 and Irs2. Although the Irs1 and Irs2 mRNA and protein levels were almost completely abrogated in the endothelial cells of the ETIrs1/2DKO mice (Figures 3G and 3H), no significant differences in the mRNA or protein levels of eNOS and ET-1 were observed between the control and ETIrs1/2DKO mice (Figures 3G and 3H). The insulin-stimulated phosphorylation levels of Akt and eNOS were significantly reduced in the ETIrs1/2DKO mice (Figure 3I). The insulin tolerance test revealed that the glucose-lowering effect of insulin was significantly attenuated in the ETIrs1/2DKO mice (Figure 3J), and the glucose tolerance test revealed significantly elevated plasma glucose levels in the ETIrs1/2DKO mice (Figure 3K). Moreover, the GIR and Rd in the ETIrs1/2DKO mice were significantly reduced as compared with the values not only in the control mice but also in the ETIrs2KO mice (Figure 3L). These data suggest that Irs1 may play a significant role in endothelial cell insulin signaling, which becomes evident especially when Irs2 expression is downregulated, such as in the ETIrs2KO and HF diet-fed mice.

Restoration of Insulin-Induced eNOS Phosphorylation in the Endothelial Cells Restored Glucose Uptake by the Skeletal Muscle in the ETIrs2KO Mice

To determine whether restoration of the insulin-induced eNOS phosphorylation in the endothelial cells might restore the glucose uptake by the skeletal muscle, we administered beraprost sodium (BPS), a stable prostaglandin $(PGI)_2$ analog (Kainoh et al., 1991), to the ETIrs2KO mice; this agent has been reported to increase the expression levels of eNOS mRNA and protein through the cyclic adenosine monophosphate (cAMP)-, protein kinase A-, and cAMP-responsive element-mediated pathways (Niwano et al., 2003). Indeed, this treatment increased the eNOS mRNA and protein expression levels in the endothelial cells (Figures 4A and 4B). BPS treatment restored insulin-induced phosphorylation of eNOS in the BPS-treated ETIrs2KO mice to a level similar to that observed in the saline-treated control mice (Figure 4B), despite the absence of any change in the ratio of phosphorylated eNOS to total eNOS (Figure 4B); also, no change in the insulin-induced phosphorylation of Akt was observed in these mice (Figure S3A). The insulin-induced increase of the capillary blood volume and interstitial concentrations of insulin were restored at 60 and 120 min after insulin infusion in the hyperinsulinemic-euglycemic clamp study (Figures 4C and 4D and data not shown) under comparable plasma insulin concentrations (Figure S3B and data not shown). The restoration of the insulin-induced increase of the capillary blood volume by BPS treatment in the ETIrs2KO mice was completely blocked by administration of the NOS inhibitor, N^G-nitro-$_L$-arginine methyl ester ($_L$-NAME) (Figure 4E), suggesting that the restoration of the insulin-induced capillary recruitment by BPS treatment was eNOS dependent. To rule out the possibility that BPS and $_L$-NAME regulated the skeletal muscle glucose uptake through an eNOS-independent mechanism, we next administered BPS and $_L$-NAME to eNOS-knockout (eNOSKO) mice. There were no significant differences in the insulin-induced increases of the capillary blood volume or interstitial insulin concentrations among the saline-treated, BPS-treated, and $_L$-NAME-treated eNOSKO mice, either at the basal

Figure 2. Irs2 Deletion in the Endothelial Cells Caused an Insulin Signaling Defect Resulting in a Reduction of the Insulin-Induced Increase of the Capillary Blood Volume and Interstitial Concentrations of Insulin and, as a Consequence, Impaired Glucose Uptake by the Skeletal Muscle

(A) Expression levels of Irs1 and Irs2 mRNA in the endothelial cells of the WT, Tie2-Cre, Irs2lox/lox, and ETIrs2KO mice (n = 4–8).

(B) The expression levels of Irs2 in the WAT, liver, and skeletal muscle of the WT, Tie2-Cre, Irs2lox/lox, and ETIrs2KO mice (n = 5–6).

(C) Insulin-stimulated tyrosine phosphorylation levels of Irβ, Irs1, and Irs2 in the endothelial cells of the ETIrs2KO mice.

(D) Phosphorylation levels of Akt and eNOS in the endothelial cells of the ETIrs2KO mice (n = 8–12).

(E and F) Capillary blood volume (E) and interstitial insulin levels (F) in the ETIrs2KO mice (n = 3–10).

(G and H) Insulin tolerance test (G) and glucose tolerance test (H) in the ETIrs2KO mice (n = 8–10).

(I) GIR, EGP, and Rd in the ETIrs2KO mice after insulin infusion in the hyperinsulinemic-euglycemic clamp study (n = 3–9).

(J) Glucose uptake by the skeletal muscle in the ETIrs2KO mice after insulin infusion in the hyperinsulinemic-euglycemic clamp study (n = 3–9).

(K) Glucose uptake by the isolated skeletal muscle in the ETIrs2KO mice (n = 3).

(L) Phosphorylation levels of Akt (ser473) in the skeletal muscle of the ETIrs2KO mice after insulin infusion in the hyperinsulinemic-euglycemic clamp study (n = 3–4). "Control" indicates $Irs2^{lox/lox}$ mice. "NA" indicates not applicable. Where error bars are shown, the results represent the means ± SEM. *$p < 0.05$, **$p < 0.01$, ***$p < 0.001$.

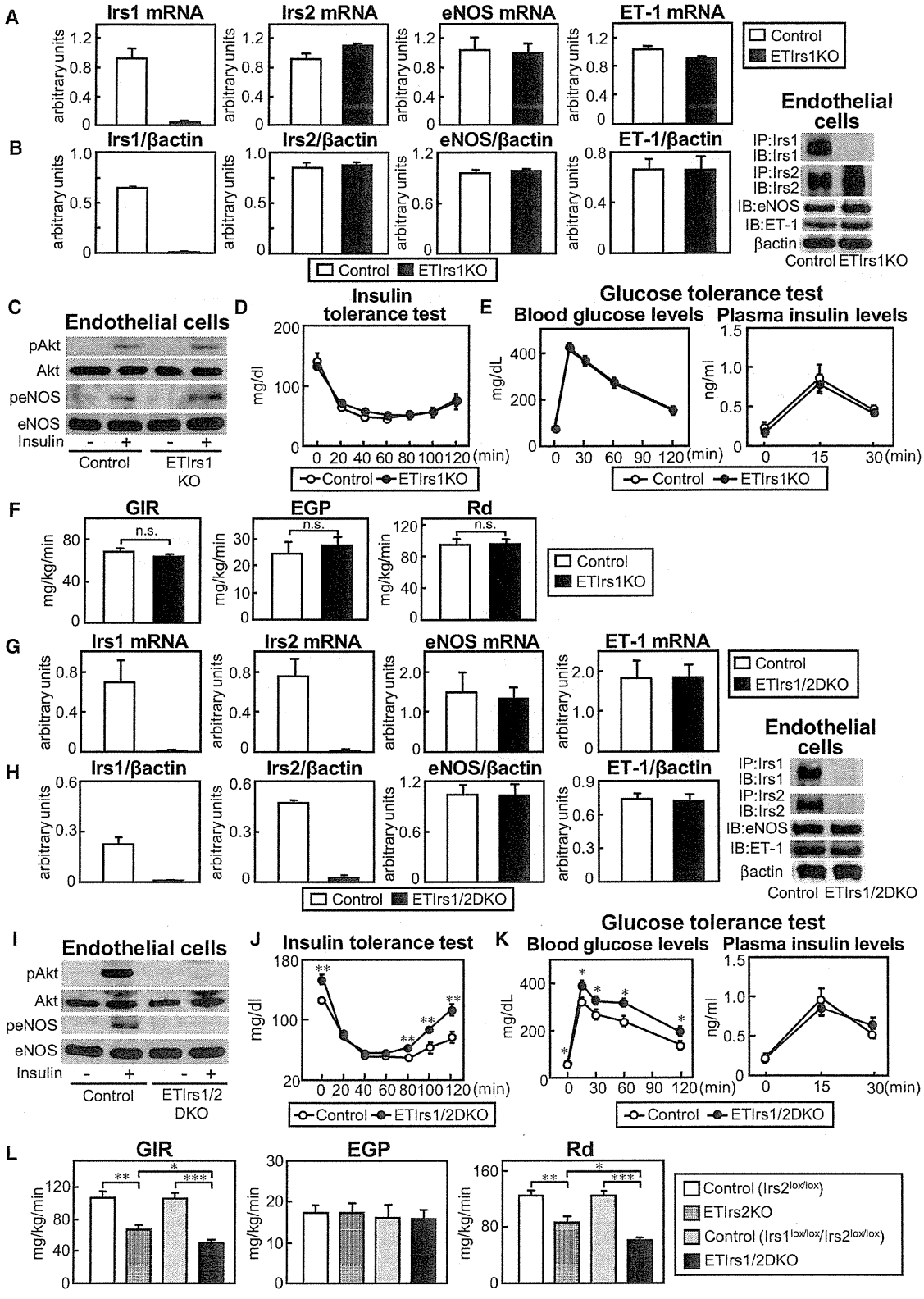

Figure 3. In the ETIrs1/2DKO, but Not ETIrs1KO, Mice, the GIR and Rd Were Significantly Reduced as Compared with the Values Seen Not Only in the Control Mice, But Also in the ETIrs2KO Mice, in Addition to the Impairment of Insulin Signaling in the Endothelial Cells, Whole-Body Insulin Sensitivity, and Glucose Tolerance

(A and B) Expression levels of Irs1, Irs2, eNOS, or ET-1 mRNA and protein in the endothelial cells of the ETIrs1KO mice (n = 3–6).

or at 60 min after insulin infusion (Figures S3C and S3D). Moreover, there were no significant differences in the results of the insulin tolerance or glucose tolerance tests, or in the skeletal muscle glucose uptake among the three groups (Figures S3E–S3G). These data strongly suggest that the effects of both BPS and L-NAME were eNOS dependent. The GIR and Rd were completely restored in the BPS-treated ETIrs2KO mice at 60 and 120 min after insulin infusion (Figure 4F and data not shown). We also measured the glucose uptake by the skeletal muscle after insulin infusion in the hyperinsulinemic-euglycemic clamp study. Glucose uptake by the skeletal muscle after insulin infusion was completely restored in the BPS-treated ETIrs2KO mice (Figure 4G). On the other hand, the glucose uptake by the isolated skeletal muscle from the BPS-treated ETIrs2KO mice remained essentially unchanged (Figure 4H), indicating the absence of any significant effect of BPS treatment on the glucose uptake by the skeletal muscle per se. Consistent with the results for the interstitial insulin concentrations, the phosphorylation levels of Irβ, as well as those of Irs1 and Akt, in the skeletal muscle were also completely restored in the BPS-treated ETIrs2KO mice at 60 min after insulin infusion into the inferior vena cava (Figure S3H). These data suggest that restoration of the insulin-induced phosphorylation of eNOS in the endothelial cells also restored the insulin-induced capillary recruitment and increase of the interstitial concentrations of insulin, consequently restoring the insulin-induced glucose uptake by the skeletal muscle. Alternatively, there is also the possibility that concomitant BPS plus insulin treatment activated eNOS via a pathway independent of the insulin/Irs/Akt pathway, even though BPS alone had no effect on eNOS phosphorylation. No significant differences were observed in the food intake, body weight, or weights of the visceral and subcutaneous fat pads among the three groups (Figure S4A). No significant differences in the plasma lipid profile or expression levels of adipokines were observed either among the three groups (Figures S4B and S4C). No significant difference in the 2-[^{3}H]DG uptake by the skeletal muscle was noted between the saline- and L-NAME-treated control mice (Figure S4D).

Restoration of Insulin-Induced eNOS Phosphorylation in the Endothelial Cells Restored the Glucose Uptake by the Skeletal Muscle in the HF Diet-Fed Mice

Could the restoration of insulin-induced eNOS phosphorylation in the endothelial cells also ameliorate the impaired glucose uptake by the skeletal muscle in the HF diet-fed obese mice? BPS treatment significantly increased the eNOS mRNA (Figure 5A) and protein (Figure 5B) expression levels. BPS treatment in the HF diet-fed mice restored insulin-induced phosphorylation of eNOS to a level similar to that observed in the saline-treated normal chow-fed mice (Figure 5B), despite the absence of any change in the ratio of phosphorylated eNOS to total eNOS in the BPS-treated HF diet-fed mice (Figure 5B); also, no change in the insulin-induced phosphorylation of Akt was observed in these mice (Figure S5A). These data suggest that restoration of the insulin-induced eNOS phosphorylation in the BPS-treated HF diet-fed mice was not due to improvement of insulin signaling, but was rather proportional to the protein expression levels of eNOS. The decreased capillary blood volume and interstitial concentrations of insulin observed in the saline-treated HF diet-fed mice were restored at 60 and 120 min after insulin infusion in the BPS-treated HF diet-fed mice (Figures 5C and 5D and data not shown), when the plasma insulin levels were adjusted to be the same among the three groups (Figure S5B and data not shown). The restoration of the capillary blood volume by BPS treatment at 60 min after insulin infusion in the HF diet-fed mice was completely blocked by L-NAME treatment (Figure 5E). Consequently, the GIR and Rd at 60 and 120 min after insulin infusion were significantly, but not completely, restored by BPS treatment, although the increased EGP remained unchanged (Figure 5F and data not shown). We also measured the skeletal muscle glucose uptake after insulin infusion in the hyperinsulinemic-euglycemic clamp study. Glucose uptake by the skeletal muscle after insulin infusion was significantly, but not completely, restored in the BPS-treated HF diet-fed mice (Figure 5G). On the other hand, the glucose uptake by isolated skeletal muscle from the HF diet-fed mice treated with BPS remained essentially unchanged (Figure 5H), indicating the absence of any significant effect of BPS treatment on the glucose uptake by the skeletal muscle per se. Consistent with the results for the interstitial insulin concentrations, the insulin-induced phosphorylation levels of Irβ, as well as those of Irs1 and Akt, in the skeletal muscle at 60 min after insulin infusion into the inferior vena cava were significantly, but not completely, restored in the BPS-treated HF diet-fed mice (Figure S5C). Moreover, the increase in the blood glucose after glucose loading was significantly, but not completely, ameliorated during an oral glucose tolerance test conducted after BPS treatment in the HF diet-fed mice (Figure S5D). No significant differences in the food intake, body weight, or weights of the visceral and subcutaneous fat pads were noted between the saline- and BPS-treated HF diet-fed mice (Figure S5E). No significant differences in the plasma lipid profile or expression levels adipokines were noted between the saline- and BPS-treated HF diet-fed mice (Figures S5F and S5G). Taken together, restoration of insulin-induced eNOS activation in the endothelial cells restored the insulin-induced capillary recruitment and interstitial insulin concentrations, resulting in improvement of the skeletal muscle glucose uptake in the HF diet-fed obese mice.

(C) Insulin-stimulated phosphorylation levels of Akt and eNOS in the endothelial cells of the ETIrs1KO mice (n = 3–5).
(D and E) Insulin tolerance test (D) and glucose tolerance test (E) in the ETIrs1KO mice (n = 6).
(F) GIR, EGP, and Rd in the ETIrs1KO mice during the hyperinsulinemic-euglycemic clamp study (n = 6–8).
(G and H) Expression levels of Irs1, Irs2, eNOS, and ET-1 mRNA and protein in the endothelial cells of the ETIrs1/2DKO mice (n = 3–6).
(I) Insulin-stimulated phosphorylation levels of Akt and eNOS in the endothelial cells of the ETIrs1/2DKO mice (n = 5–6).
(J and K) Insulin tolerance test (J) and glucose tolerance test (K) in the ETIrs1/2DKO mice (n = 8–9).
(L) GIR, EGP, and Rd in the ETIrs1/2DKO mice during the hyperinsulinemic-euglycemic clamp study (n = 5–10). "Control" of ETIrs1KO mice indicates $Irs1^{lox/lox}$ mice; "Control" ETIrs1/2DKO mice indicates $Irs1^{lox/lox}/Irs2^{lox/lox}$ mice. Where error bars are shown, the results represent the means ± SEM. *$p < 0.05$, **$p < 0.01$, ***$p < 0.001$.

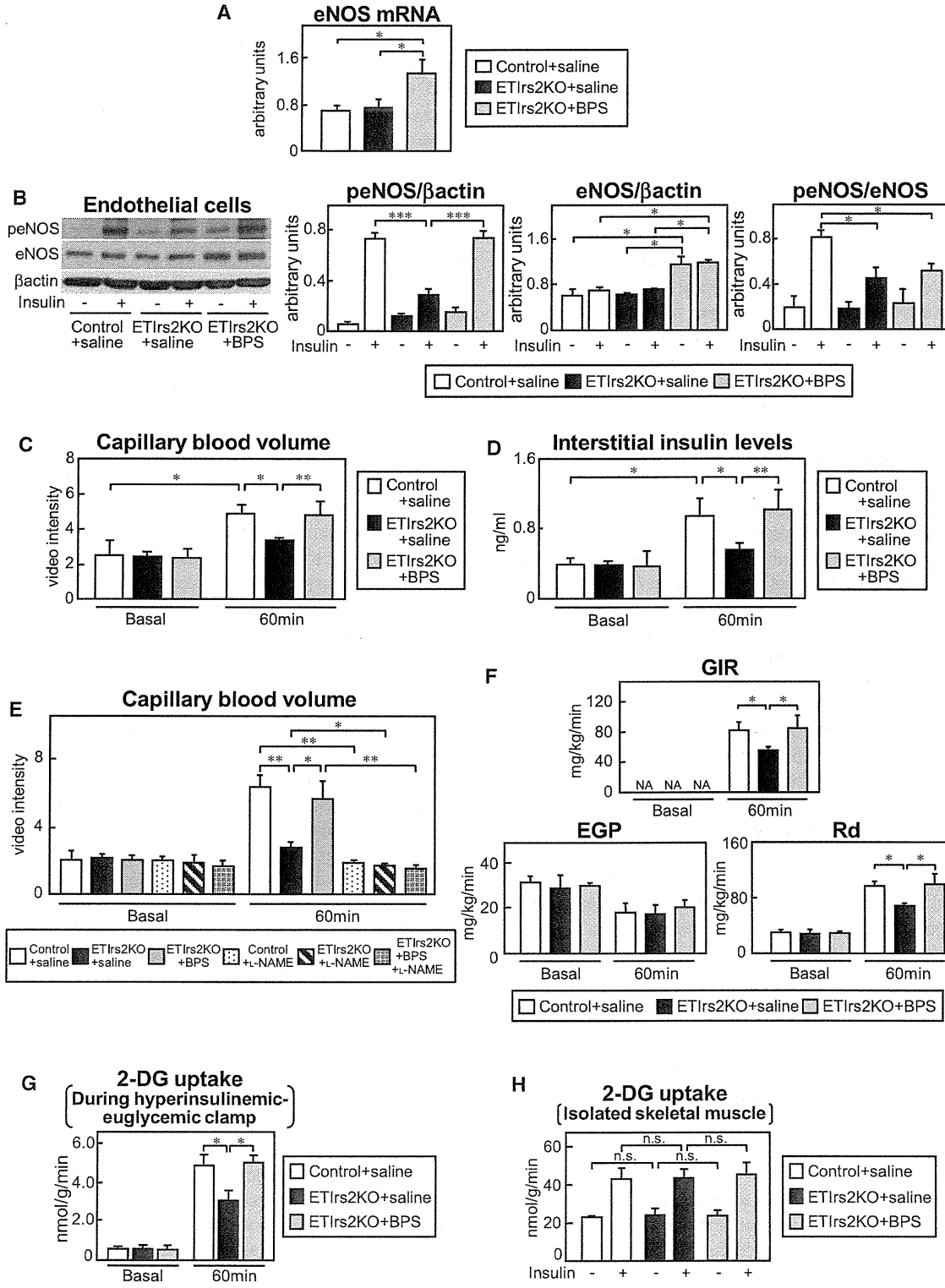

Figure 4. Restoration of the Insulin-Induced Phosphorylation of eNOS in the Endothelial Cells Restored the Insulin-Induced Increase of the Capillary Blood Volume and Interstitial Concentrations of Insulin; as a Consequence, the Insulin-Induced Glucose Uptake by the Skeletal Muscle Was Also Restored in the ETIrs2KO Mice

(A–D) eNOS mRNA levels (A), insulin-stimulated phosphorylation level of eNOS (B), capillary blood volume (C), and interstitial insulin concentrations (D) in the BPS-treated ETIrs2KO mice (n = 5–8).

(E) Capillary blood volume in the BPS-treated ETIrs2KO mice following $_L$-NAME treatment (n = 4–6).

DISCUSSION

In this study, we demonstrated that endothelial insulin signaling is also significantly impaired in HF diet-fed mice, as in the other target organs of insulin, such as the liver and skeletal muscle. Moreover, insulin-induced capillary recruitment, increase of interstitial insulin concentrations, and glucose uptake were also significantly decreased in the skeletal muscle, all of which were reversed by restoration of the insulin-induced phospholyration of eNOS in the endothelial cells. These data suggest that impaired insulin signaling in the endothelial cells, with reduction of Irs2 expression and insulin-induced eNOS phosphorylation, reduces insulin-induced glucose uptake by the skeletal muscle via, at least in part, decreased capillary recruitment and decreased interstitial insulin concentrations in the skeletal muscle. In fact, an insulin signaling defect induced by Irs2 deletion from the endothelial cells caused impaired insulin-induced glucose uptake by the skeletal muscle, along with attenuation of the insulin-induced capillary recruitment and increase of interstitial insulin concentrations.

Based on these data, we provide insight into the mechanism of insulin resistance in the skeletal muscle (Figure 6). Since the plasma insulin levels of lean subjects are low, and the expression levels of Irs2 in their endothelial cells are presumably maintained under the fasting condition, insulin-mediated Akt and eNOS activations are induced optimally after feeding, resulting in insulin-induced capillary recruitment, increase of interstitial insulin concentrations, and increase of glucose uptake by the skeletal muscle. By contrast, since downregulation of Irs2 expression is probably induced by hyperinsulinemia in the endothelial cells of obese subjects, the insulin-mediated Akt and eNOS activations after feeding are inadequate, and as a result, insulin-induced capillary recruitment, increase of interstitial insulin concentrations, and increase of glucose uptake by the skeletal muscle are impaired in obese subjects. This insight into the mechanism also sheds light on the physiological roles of Irs2 in the endothelial cells. Expression of a sufficient amount of Irs2 in the endothelial cells appears to be critical to normal glucose homeostasis. When Irs2 expression is abundant in the fasting state, adequate glucose uptake by the skeletal muscle is induced and the elevated glucose levels return to within the normal range after feeding. However, when Irs2 expression in the endothelial cells is reduced in the fasting state in the presence of hyperinsulinemia with insulin resistance, insulin signaling is impaired, and the elevated glucose levels after feeding fail to decrease efficiently, and in fact, the ETIrs2KO mice actually exhibited glucose intolerance in the glucose tolerance test (Figure 2H).

Insulin normally induces both vasorelaxation and vasoconstriction: insulin-induced vasorelaxation is mediated by the Irs-PI3K-Akt pathway increasing endothelial NO production, and insulin-induced vasoconstriction is mainly mediated by the Shc/SOS/Ras-MAPK pathway inducing ET-1 expression (Muniyappa and Quon, 2007). While insulin-induced eNOS activation was significantly decreased in the endothelial cells of both the ETIrs2KO and ETIrs1/2DKO mice (Figures 2D and 3I), the ET-1 expressions remained unchanged in both models in this study, indicating that insulin signaling was selectively impaired in the endothelial cells of these mice (Figures 3G and 3H; Figures S2A and S2B). This selective insulin signaling defect appears to be critical to the impairment of the insulin-induced glucose uptake by the skeletal muscle. In fact, endothelial-cell-specific insulin receptor-knockout (VENIRKO) mice, in which both the Irs-PI3K-Akt-eNOS and Shc/SOS/Ras-MAPK-ET-1pathways are disrupted, do not exhibit skeletal muscle insulin resistance (Vicent et al., 2003). Moreover, King et al. demonstrated that while the MAPK activity in the microvessels of obese Zucker rats remained unchanged, the Irs1 protein and Irs1-associated PI3kinase activity were modestly reduced, and the Irs2 protein and Irs2-associated PI3kinase activity were reduced even further (Jiang et al., 1999). Furthermore, VENIRKO mice developed insulin resistance when fed either low- or high-salt diets. These data suggest that the Irs-PI3K-Akt pathway may be more susceptible to the adverse effects of conditions such as obesity and dietary salt intake.

ETIrs2KO mice showed glucose intolerance, insulin resistance, and impaired glucose uptake by the skeletal muscle in vivo (Figures 2G–2J), despite the skeletal muscle per se not showing impaired insulin-induced glucose uptake (Figure 2K). In contrast, although myocyte-specific insulin receptor-knockout mice exhibited impaired glucose uptake by the skeletal muscle per se, as glucose uptake by insulin was decreased in the isolated skeletal muscle, the glucose tolerance and insulin sensitivity were almost normal in vivo (Brüning et al., 1998). Why did the ETIrs2KO, but not MIRKO, mice show skeletal muscle insulin resistance in vivo? It has been reported that there are mainly two different pathways of physiological glucose uptake by the skeletal muscle: one mediated in an insulin-dependent manner, such as after a meal, and the other in an insulin-independent manner, such as during exercise (Clark, 2008). Considering the phenotype of the MIRKO mice, the glucose uptake in the myocytes showing defective expression of the insulin receptor throughout growth and development may be largely compensated for by insulin-receptor-independent glucose uptake mechanisms. There may be little such compensatory mechanisms for glucose uptake in the ETIrs2KO mice, which show adequate expression of the insulin receptor in the skeletal muscle. Consequently, these mice may exhibit impairment of insulin-induced glucose uptake by the skeletal muscle, unlike the MIRKO mice.

To what degree is the impaired insulin delivery induced by the endothelial insulin signaling defect involved in the skeletal muscle insulin resistance in obesity and type 2 diabetes? Glucose uptake by the skeletal muscle was restored by 50% or more with improvement of the endothelial insulin signaling and insulin delivery in HF diet-fed mice (Figures 5B and 5G).

(F) GIR, EGP, and Rd in the BPS-treated ETIrs2KO mice after insulin infusion in the hyperinsulinemic-euglycemic clamp study (n = 4–8).
(G) Glucose uptake by the skeletal muscle in the BPS-treated ETIrs2KO mice after insulin infusion in the hyperinsulinemic-euglycemic clamp study (n = 4–8).
(H) Glucose uptake by the isolated skeletal muscle in the BPS-treated ETIrs2KO mice (n = 3–6). "NA" indicates not applicable. Where error bars are shown, the results represent the means ± SEM. *$p < 0.05$, **$p < 0.01$, ***$p < 0.001$.

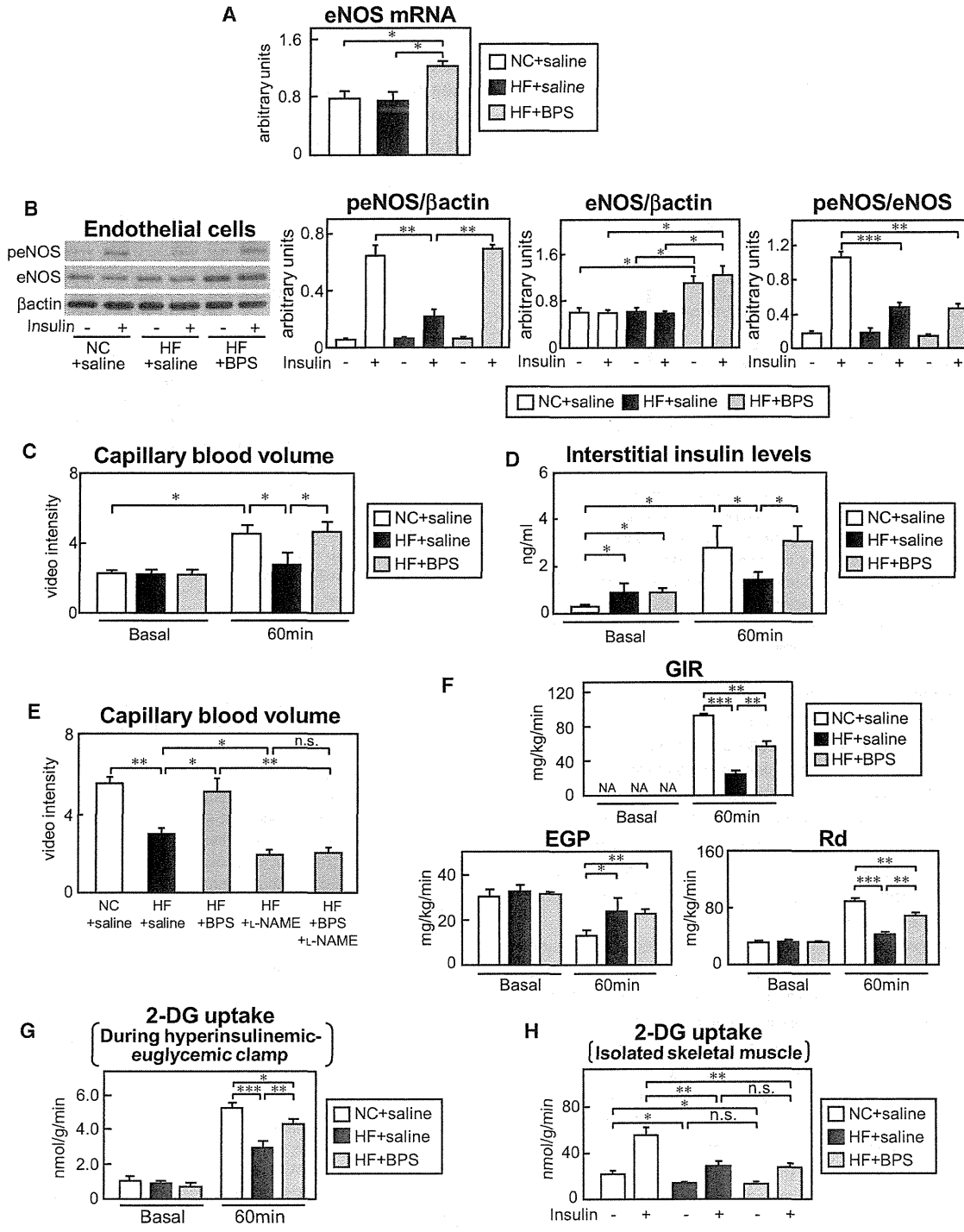

Figure 5. Restoration of the Insulin-Induced Phosphorylation of eNOS Restored the Insulin-Induced Increase of the Capillary Blood Volume and Interstitial Insulin Concentrations, Resulting in Improvement of the Glucose Uptake by the Skeletal Muscle in the HF Diet-Fed Obese Mice

(A–D) eNOS mRNA levels in the endothelial cells (A), insulin-stimulated phosphorylation level of eNOS (B), capillary blood volume (C), and interstitial insulin concentrations (D) in the BPS-treated HF diet-fed mice (n = 5–8).

(E) Capillary blood volume in the BPS-treated HF diet-fed mice following L-NAME treatment (n = 4–6).

(F) GIR, EGP, and Rd in the BPS-treated HF diet-fed mice after insulin infusion in the hyperinsulinemic-euglycemic clamp study (n = 3–5).

(G) Glucose uptake by the skeletal muscle in the BPS-treated HF diet-fed mice after insulin infusion in the hyperinsulinemic-euglycemic clamp study (n = 3–5).

(H) Glucose uptake by the isolated skeletal muscle in the BPS-treated HF diet-fed mice (n = 3–5). "NC" indicates normal chow-fed mice. "NA" indicates not applicable. Where error bars are shown, the results represent the means ± SEM. *$p < 0.05$, **$p < 0.01$, ***$p < 0.001$.